CrystEngComm

Accepted Manuscript

Correlating the melting point alteration with the supramolecular structure in Aripiprazole drug cocrystals.

Jagadeesh Babu Nanubolu* and Krishnan Ravikumar*

[a]Centre for X-ray Crystallography, CSIR-Indian Institute of Chemical Technology, Hyderabad, India, 500607. Corresponding authors: E-mail: jagadeesh81@gmail.com and sshiya@yahoo.com Telephone: +91 (0) 4027193118 Fax +91 (0)4027193118.

Electronic supplementary information (ESI) available: CIF files, IR data table, ESP plot, PXRD comparison, TGA plots and crystal packing diagrams of IV and V.

Abstract

Five novel cocrystals of antipsychotic drug aripiprazole are reported with dihydroxy- and trihydroxybenzene coformers. Co-crystals are designed by exploiting the piperazine N acceptor of aripiprazole to involve in O–H···N hydrogen bonding with the hydroxyl functional group of coformers. Powder X-ray diffraction, IR spectroscopy, single crystal X-ray diffraction, Differential Scanning Calorimetry and Thermo Gravimetric Analysis are employed for the characterization of new solid forms. Significant changes are noted in the melting points of cocrystals even though the coformers are similar in size and have adopted isostructural crystal packing with aripiprazole. For example, aripiprazole-catechol cocrystal melts at 121.2°C whereas its isostructural aripiprazole-resorcinol partner melts at 175.6°C. Plausible reasons accounting for the thermal differences are inferred from a combined single crystal and spectroscopic study. Our results indicate that higher melting cocrystals are noticed in structures sustained by strong helical networks of O–H···N and O–H···O hydrogen bonds along the three dimensional space in the crystal. Lower melting cocrystals are noticed when strong hydrogen bonds are restricted to two dimensional layers leaving their three dimensional interlayer packing achieved by weaker interactions. The presence of stronger hydrogen bonds in higher melting cocrystals is also evidenced by amide spectral shifts. The isostructurality in cocrystals is an advantage in this study for it had allowed a direct structural comparison in different cocrystals and accounted for their thermal behaviour.

Introduction

The melting point is a fundamental physical property which is determined by the temperature at which the solid phase is at equilibrium with the liquid phase.[1] High melting points are usually desirable for stability and processing of pharmaceuticals and agrochemicals.[2] As a result, the melting point alteration becomes an important step as a part of the drug formulation and development. Traditional synthetic procedures rely on a covalent bond modification approach to alter the melting behavior. The non covalent derivatization,[3] popularly known as co-crystallization, is an alternative approach to modify the physicochemical properties without the need to break /or make covalent bond linkages. The co-crystallization principle involves homogeneous mixing of the target molecule with an auxiliary molecule such that they interact with each other by intermolecular interactions in a well defined stoichiometric ratio and together form a favorable cocrystal lattice.[4] Both the reactants are fully incorporated into the product cocrystal lattice, thus virtually no waste is generated. Unlike molecular salts which involve a clear proton transfer from the acid to base functional group, co-crystals are neutral complexes,

stabilized in the same crystal lattice by various non-covalent interactions such as hydrogen bonds, π… π interactions, halogen bonds, van der Walls forces and etc.[5] Over the last decade, co-crystals have gained enormous importance in the pharmaceutical and agrochemical community because of their ability to enhance the dissolution rates, equilibrium solubility, chemical stability and mechanical properties by many folds.[6,7]

A statistical study by Schultheiss et al[8a] on 50 cocrystal systems indicated that, majority of cocrystals (26/50, 51%) had melting points in between those of the drug and coformer, 19/50 (39%) were lower than either the drug or coformer, 2/50 (4%) had the same melting point as either the drug or coformer and only 3/50 (6%) were higher than both the drug and coformer. While these studies on cocrystals have shown the melting point enhancements or depression by co-crystallization method,[8] the exact reasons for melting point variations are poorly understood and are mostly linked with the coformer melting points. In this contribution, we present a novel cocrystal system consisting of antipsychotic drug aripiprazole with five phenolic coformers (scheme 1), exhibiting higher, intermediate and lower melting points than the drug and coformers. A cocrystal system showing all three variations is a rare observation which has prompted us to investigate this system more in detail to understand any underlying structural features responsible for the observed melting points. Establishing structure-property connections in multi-component systems is more challenging, because co-crystallizing systems can interact in different ways resulting in different stoichiometry, space groups and packing.[8a] Fortunately, in the present study, four out of five cocrystals are found to be isostructural, meaning they maintained the 1:1 drug to coformer ratio and crystallized in the same space group with identical unit cell dimensions and crystal volume. Nevertheless these isostructural cocrystals displayed significant melting points over a broad temperature range 120-180°C and allowed for a direct structural comparison.

We were initially motivated to undertake co-crystallization attempts on aripiprazole because the drug was known to crystallize in eight polymorphic forms,[9] a hydrated form[9a] and ten salt forms,[10] but cocrystals have not been reported till date in the Cambridge Structural Database.[11] This is the first cocrystal report on aripiprazole describing the design principles for cocrystal formation and structure-property connections. We employed powder X-ray diffraction (PXRD), solid state FT-Infrared spectroscopy (IR), Differential Scanning Calorimetry (DSC), Thermo Gravimetric Analysis (TGA) and single crystal X-ray diffraction techniques for cocrystal characterization.

Experimental Section

Materials: Prior to setting up various crystallizations, Aripiprazole (gift sample from Mylan Laboratories, Hyderabad) was recrystallized from EtoAC and was identified as pure single phase by PXRD and SC-XRD. Phenolic compounds resorcinol, catechol, hydroquinone, pyrogallol and phloroglucinol (HiMedia, Hyderabad) were used directly in co-crystallization experiments.

Crystallizations: Slow evaporation method was employed for growing crystals. Equimolar mixtures of aripiprazole (50mg, 0.1115 mmol) with five coformers (resorcinol, 12.28 mg; catechol, 12.28mg; hydroquinone, 12.28mg; pyrogallol, 14.06mg; phloroglucinol, 14.0gmg, 0.1115 mmol) were dissolved in a suitable solvent or mixture of solvents and allowed to re-crystallize at room temperature. Good quality crystals of aripiprazole cocrystals with resorcinol (I) and pyrogallol (IV) were grown from methanol. Co-crystallization attempts with catechol, hydroquinone and phloroglucinol in methanol, ethanol or any other polar solvents mostly resulted in phase separation and yielded aripiprazole monohydrate. After several crystallization attempts by varying solvents and solvent combinations, we could grow cocrystals of aripiprazole with catechol (III) from toluene, with hydroquinone (III) from benzene and with

phloroglucinol (V) from benzene-ethyl acetate solvent mixture in equal volumes. The aripiprazole-coformer stoichiometric ratio in all cocrystals was 1:1. Solid state grinding method[5] was also employed for cocrystal formation. Equimolar mixtures were ground in mortar using pestle for 10 minutes and few drops of methanol was used for lubrication. The material was reground for another 10 minutes and allowed dry at room temperature in the open atmosphere for 12 hours. The grounded materials were confirmed as new cocrystal phases by powder X-ray and IR spectroscopy.

Powder X-ray diffraction (PXRD): The PXRD patterns were recorded at room temperature using a Bruker diffractometer with Cu Kα radiation (λ = 1.5418 Å), running at 40Kv and 30Ma. The 2θ range was covered from 2.00 to 50.00 degrees with a step size of 0.005 degree. Smoothing factor of 0.08 was used for correcting the baseline noise levels in the Bruker EVA program.[12a] PowDLL version 2.25.4315.30639[12b] was used for converting the Bruker Raw data to XY format. Simulated powder X-ray diffraction patterns from the single crystal X-ray data were generated in the CCDC mercury software 2.4 (Build RC5) using "powder pattern" module.[12c] X-ray wavelength was set as 1.54060Å with 2θ range 2-50°, a step of 0.005° and FWHM (2θ) as 0.1. The plotting program XMGrace[12d] was used for preparing off-stack PXRD plots.

Spectroscopic measurements: FT-IR spectra were recorded on solid samples using Perkin Elmer 100 FT-IR spectrometer using pressed KBr disc method. A finely ground 1% mixture of a solid sample in KBr (~2 mg of the sample is dispersed in 200mg of KBr) is fused into a transparent disc using a hydraulic press. The spectra were collected on the fused discs in the spectral range 400-4000 cm^{-1} by averaging 108 scans with a spectral resolution of 4 cm^{-1}. The spectra were saved in XY format, normalized in Labspec software version 5.54.15 (Horiba Jobin Vyon, Japan)[12e] and plotted in Xmgrace.[12d]

Thermal measurements: Differential scanning calorimetry (DSC) studies were performed on Mettler Toledo DSC-1 STAR[e] instrument. Approximately 5mg of compound was taken sealed pans and the samples were heated from room temperature to 220°C with a 5°C per minute heating rate. Thermo gravimetric analyses (TGA) of cocrystals were recorded on Mettler Toledo TGA/SDTA 851[e] instrument. The melting points of the cocrystals and their starting materials were also confirmed on a digital melting point apparatus (model No. CONTECH CDMP-300-01). A small quantity of the material was filled into the capillaries and was heated at 5°C per minute heating rate. The observed melting points of parent compounds are in accordance with the reported values in literature.[13]

Single crystal X-ray diffraction (SC-XRD): The intensity data were collected at room temperature using a Bruker Smart Apex CCD diffractometer with graphite monochromated Mo-Kα radiation (λ=0.71073Å) by the ω-scan method. Preliminary lattice parameters and orientation matrices were obtained from four sets of frames. Unit cell dimensions were determined using 6098, 6927, 4076, 7629, 8444 reflections in cocrystals I, II, III, IV and V, respectively. Integration and scaling of the intensity data were accomplished using the program SAINT.[14a] The structures were solved by direct methods using SHELXS97 and refinement was carried out by full-matrix least-squares technique using SHELXL2014/7.[14b-c] Anisotropic displacement parameters were calculated for all non-hydrogen atoms. All N-bound and O-bound H atoms were located in the difference Fourier density map and refined isotropically. The C-bound H atoms were located in difference density maps but were positioned geometrically and included as riding atoms, with C—H = 0.93–0.98 Å , and with $U_{iso}(H) = 1.5U_{eq}(C)$ for methyl H atoms and $1.2U_{eq}(C)$ otherwise. The hydroxyl group on the catechol ring in cocrystal II is disordered over two sites with an occupancy factor of 0.624(8) for major (O4/C24/C29) and 0.376(8) for minor (O4D/C24D/C29D) components. Similarly, the phloroglucinol ring in cocrystal V is disordered over two sites with an occupancy factor of 0.564(2) for major (C24-C29/O3/O4/O5) and 0.436(2) for minor (C24D-

C29D/O3D/O4D/O5D) components. The anisotropic displacement parameters of the disordered carbon and oxygen atoms were restrained to be similar with EADP instruction. The C–C and C–O bond distances of the disordered atoms were restrained with DFIX instruction to a set target value of 1.38(2) and 1.40(2) Å, respectively. In hydrated cocrystals, water is partially occupied with oxygen atom occupancy refined to 0.293(9) in cocrystal II and 0.256(5) in cocrystal IV. In cocrystal V, water is fully occupied but disordered over two sites with an occupancy of 0.564(2) and 0.436(2) for O6W and O6D atoms, respectively. The H atoms on water oxygen could not be located. In the disordered structures of II and V, the hydroxyl H atoms were located in difference Fourier map and refined as riding with U_{iso}(H) = 1.5 U_{eq}(O) with constrained O-H bond distances. Hydrogen bonding tables were prepared using PLATON[14d] and molecular graphics were drawn using X-Seed.[14f]

Hirshfeld surface analysis: Hirshfeld surface maps are generated in the CrystalExplorer.[15a] The difference between the molecular and hirshfeld surfaces is that the former is defined only by the molecule; while the latter is defined by the molecule and the proximity of its nearest neighbours, and hence encodes information about intermolecular interactions in the crystal.[15b-c] The default d_{norm} property is mapped onto the surface which is the normalized contact distance defined in terms of d_e (distance from a point on the surface to the nearest nucleus outside the surface), d_i (distance from a point on the surface to the nearest nucleus inside the surface) and the van der Waals radii of atoms.

Results and Discussion

Design principles

The calculated electrostatic surface potential values of aripiprazole[9c] (Fig.S1 of ESI) indicate the donor group strengths in the order, amide N-H (+358.9 KJ mol^{-1}) > aromatic C-H (+230.7 KJ mol^{-1}) > alkyl C-H (+198.8 KJ mol^{-1}) and acceptor group strengths in the order, amide C=O (-226.8 KJ mol^{-1}) > piperazine N-butyl (-204.4 KJ mol^{-1}) > piperazinyl N-phenyl (-174.3 KJ mol^{-1}) > ether O (-139.9 KJ mol^{-1}). The strongest donor-acceptor pair, amide N-H and C=O, are found to interact with each other in eight polymorphic crystals of aripiprazole[9] and result as amide N–H···O dimer or N–H···O catemer (scheme 2). However, the second strongest acceptor piperazine N-butyl was mostly unutilized or involved in weak C-H···N interactions due to the lack of a second strong donor. We reasoned that including hydroxyl compounds as "coformers" can facilitate stronger phenol···piperazine interactions with aripiprazole and help them to co-crystallize. Accordingly, five aromatic hydroxyl compounds were chosen for co-crystallization experiments (scheme 1). Guided by the quantitative pKa rule by Cruz-Cabeza,[16] we expected cocrystals over salts (scheme 2), as the estimated ΔpKa values for complexes fall in the negative ΔpKa range where the probability for cocrystal formation is 99.1% (ΔpKa = -1.59, I; -1.64, II; -2.29, III; -1.33, IV; -0.39, V).

PXRD and IR inference

At first, we employed solid state grinding approach for cocrystal formation. Equimolar mixtures of aripiprazole and phenolic coformers were weighed and ground in five separate experiments (see Experimental section). Two events can predominantly occur during the grinding process – either the reactants do not interact resulting in a physical mixture or bind with each other to form a new product cocrystal phase. Gratifyingly, all grounded materials showed distinct powder XRD patterns from the parent compounds[9,11] (Fig. 1). The new cocrystal phases of aripiprazole are labeled as I with resorcinol, II with catechol, III with hydroquinone, IV with pyrogallol and V with phloroglucinol coformers. Amongst these, cocrystals I, II, IV and V have very similar patterns in the lower 2θ angles 5-15° suggesting them to be isostructural whereas cocrystal III is different with distinct peaks. We have recorded the solid state Infrared spectra to understand vibrational changes upon cocrystal formation. As expected, distinct IR spectra are seen for cocrystals compared to parent compounds (Fig.2 and Table S1 of ESI). The intense

amide C=O peak in aripiprazole at 1679 cm^{-1} is found to be shifted in cocrystals to 1653 in I, 1673 in II, 1662 in III, 1652 in IV, and 1652 cm^{-1} in V (Fig. 2b). These shifts are attributed to the participation of carbonyl group in stronger hydrogen bonding[17] in cocrystals. Similarly, the amide N–H stretch seen at 3467 cm^{-1} in aripiprazole is shifted towards a lower frequency value in cocrystals (3298, I; 3316, II; 3319, III; 3295, IV; and 3289 cm^{-1}, V). The O–H stretches of phenolic coformers have appeared mostly as broad bands (Fig.2).

Thermal data

Differential Scanning Calorimetry (DSC) studies were performed on five crystalline solid forms to obtain the Melting point (M.P.) data. Cocrystals, capable of existing as a discrete species in equilibrium with a liquid of the same composition, exhibited characteristic sharp melting points at 175.6°C in I, 121.2°C in II, 138.4°C in III, 176.4°C in IV and 180.0°C in V. These values are different from the melting points of parent aripiprazole and phenolic coformers (Fig. 3a). A widely accepted notion is that the melting points of cocrystals correlate well with the melting points of coformers.[8a] As per this rule, higher melting cocrystals are to be expected from higher melting coformers and lower melting cocrystals from lower melting coformers. However, in the present case, the lower melting coformers (resorcinol, pyrogallol) resulted as higher melting cocrystals I and IV and higher melting coformer (hydroquinone) resulted as a lower melting cocrystal III. Cocrystals II and V showed an intermediate melting point in between the drug and coformer (Fig. 3b). The deviation in three cocrystals is clearly indicated by a poor regression coefficient R^2 value = 0.1085 on a correlation plot between M.P of cocrystal and coformer (Fig. 3c).

Certainly there must be reasons for this unexpected thermal behaviour in cocrystals. When the molecular size/shape of coformers are considered (scheme 1), the position of the hydroxyl groups on the aromatic ring appears to have a some influence on the melting points, as the coformers with hydroxyls at 1,3- positions (resorcinol, pyrogallol, phloroglucinol) resulted as higher melting cocrystals whereas 1,2- and 1,4- hydroxyl positions (catechol and hydroquinone) resulted as lower melting cocrystals. And surprisingly, the trihydroxyl coformers of IV and V and the dihydroxyl coformer of I showed similar melting points, although these coformers differ by one hydroxyl group. The exact reasons are immediately not clear. The differences in the number of hydroxyl groups and their positions on the aromatic ring can have a significant influence on the overall crystal packing. Especially, the hydrogen bonds formed by coformer molecules with aripiprazole can play a crucial role in serving to constrain the motion of the molecules in the solid state and influence the melting points.[1,8] When the IR data is interpreted in the context of favorable hydrogen bonds, it is observed that the carbonyl peak in all high melting cocrystals I, IV and V appeared at a lower wavenumber (1652 cm^{-1}) compared to lower melting cocrystals II (1673 cm^{-1}) and III (1663 cm^{-1}), fig. 2b. Such greater shifts may be attributed to stronger hydrogen bonding in higher melting cocrystals.

Need for single crystal XRD studies

In order to fully understand these cocrystal systems, we have attempted to grow crystals of all five cocrystal systems and subjected them to single crystal X-ray diffraction analysis. Our primary objectives are to address the following; first to unambiguously confirm the cocrystal formation and the presence of neutral interactions, second to study the drug-coformer stoichiometry, third to understand conformational, hydrogen bonding and crystal packing features, and fourth to point out possible structural evidences that account for the melting point alterations in cocrystal systems. Slow evaporation method was employed for growing cocrystals of all five systems in suitable solvents (see experimental section). The crystal data is given in table 1. Single crystal data of cocrystals were used to simulate the PXRD patterns and compared with the experimental PXRD patterns. A very good correlation was noticed between the simulated and the experimental PXRD patterns of the bulk

cocrystal materials (Fig. S2 of ESI), confirming the identity of the two. Out of five novel cocrystals of aripiprazole, cocrystals IV and V can be considered as pharmaceutical cocrystals[4-7] because the respective coformers are approved by Food and Drug Administration (FDA)'s EAFUS (everything added to food, US) and GRAS (generally regarded as safe) databases.[18]

Structural features

Cocrystals I, II, IV and V crystallized in the monoclinic space group, $P2_1/c$, with almost identical unit cell dimensions (Table 1). Whereas cocrystal III crystallizes in the triclinic space group, $P\bar{1}$, and differs from the rest. Fig. 4 represents the asymmetric unit of cocrystals I-V. All cocrystals are observed in 1:1 stoichiometric ratio of aripiprazole with the respective phenolic coformers. Cocrystals I and III are anhydrate structures. Cocrystals II and IV are partially occupied hydrated structures with water oxygen site occupancy refined to 0.29 and 0.30 respectively in their crystal lattice whereas cocrystal V is a full hydrate. TGA and DSC analysis confirmed the water loss in the temperature range 30-80°C in cocrystal V (Fig.3a, Fig. S3e of ESI) and is concomitant with the melting in cocrystals II and IV (Fig. S3b, Fig. S3d of ESI). The absence of proton migration from the coformers to aripiprazole was unambiguously confirmed by locating the H atom on hydroxyl O atom (Fig. 5) and also by geometrical data comparison with known coformer structures. The typical C-O bond distance in neutral phenol is about 1.36±0.01Å in the CSD whereas it is 1.32±0.01Å in phenolate ion.[11] All phenolic coformers hydrogen bonded with aripiprazole show C-O bond distances in the range 1.35-1.37 Å suggesting them to be neutral molecules. Aripiprazole molecule is in extended conformation in I, II, IV and V, but twisted in III. An overlay of five conformations is shown in fig. 6. The conformational twist takes place along the butoxyl chain linker (O2-C10-C11-C12). The atoms O2 and C12 are oriented *anti* to each other in I [-177.9(1)°], II [-178.6(2)°], IV [-177.8(1)°)] and V [-177.7(3)] whereas oriented *gauche* in III [-67.1(3)°], as shown by Newman projection plots in fig.6. An intramolecular C–H···Cl interaction positions the orientation of phenyl ring to piperazine ring (Table 1). Intermolecular interactions stabilizing the multi component systems in cocrystals are discussed now.

In cocrystal I, the hydroxyl at position 1 of resorcinol forms O–H···N hydrogen bond with the piperazine of aripiprazole (O3-H3O···N2) and the hydroxyl at position 3 forms O–H···O hydrogen bond with the amide carbonyl O atom (O4–H4O···O1). These two interactions repeat in the crystal and form a strong hydrogen bonded helical network along the *b*-axis (Fig.7a). Aripiprazole forms a centrosymmetric N–H···O amide dimer motif with its inversion related aripiprazole and is extended into a two dimensional (2D) layer through C–H···O, C–H···π and C–H···Cl interactions with phenolic coformers (C14–H14B···Cg1, C16–H16A···O4, C8–H8···O3, C22–H22···Cl1, Fig.7b). The hydroxyls of coformers point out from the 2D layer structure and connect similar layers above and below by O–H···O and O–H···N hydrogen bonds in a helical fashion (Fig.7c). In addition, short Cl1···O1 contacts[19] between amide and chlorophenyl ring stabilize the interlayers.

In cocrystal II, the hydroxyl at position I forms O–H···N hydrogen bond with piperazine similar to cocrystal I (O3–H3O···N1), whereas the hydroxyl at position 2 does not form intermolecular O–H···O hydrogen bond with amide carbonyl O. It is involved in an intramolecular O4–H4O···O3 hydrogen bonding with the adjacent hydroxyl and an intermolecular O4–H4O···O5W contact with the water (Fig.4b). The amide of aripiprazole forms a centrosymmetric N–H···O dimer motif which is extended into a layered structure by C–H···π, C–H···O and C–H···Cl interactions (C14–H14B···Cg1, O5–H5O···N1, C8–H8···O3 and C8–H8···O4, Fig.8a). Additionally, water hydrogen bonds with hydroxyl and chlorine atoms (O4–H4O···O5W, Cl2···O5W) stabilize the layer. Short Cl1···O1 contacts and O3–H3O···N1 connect the interlayers (Fig.8b). Overall, the crystal packing in cocrystal II is weaker compared to I, because of O–H···O hydrogen bonding between amide O and hydroxyl resulting in a helical networking is missing.

In cocrystal III, the amide of aripiprazole forms a centrosymmetric N–H···O dimer which results in a discrete unit though O–H3O···N1 and O4–H4O···O1 interactions (Fig.9a). All the available strong H-bond donor/acceptor groups have been utilized within this discrete unit, leaving the two and three dimensional crystal packing essentially governed by weaker C–H···π, C–H···Cl and C–H···O contacts (C17–H17A···Cl1, C3–H3B···Cg1, C2–H2A···O2, Fig.9b-c).

Cocrystals IV and V displayed both helical networking and layered arrangements similar to cocrystal I. The helices are formed by O3–H3O···N2 and O5–H5O···O1 interactions along the b-axis (cocrystal IV, Fig.10a; cocrystal V, Fig.10b). The centrosymmetric N–H···O dimers extend into layers by C–H···π, C–H···O and C–H···Cl interactions (C14–H14B···Cg1, C8–H8···Cg2, C16–H16A···O5, C8–H8···O3, C22–H22···Cl1 in cocrystal IV (Fig. S4a of ESI); C14–H14B···Cg1, C16–H16A···Cg2, C17–H17B···O4, C8–H8···O3, C22–H22···Cl1 in cocrystal V (Fig.S4b of ESI, table 1). Water forms hydrogen bonds within the layer and interlayers in cocrystal IV (O4–H4O···O5W, Cl2···O6W, O3···O6W, Fig. S5a) whereas it is only involved along the interlayers in cocrystal V (O4–H4O···O6W, Fig. S5b). Short Cl1···O1 contacts are also seen between the layers similar to cocrystal I.

To briefly summarize the structural aspects, cocrystals I, IV and V showed isostructural crystal packing (Figs. 7, 8, 10, S4, S5). They formed similar 2D layers by amide N-H···O dimer, C–H···O, C–H···π, C–H···Cl interactions & interlayer helical networking by O–H···N and O–H···O hydrogen bonds. The trihydroxyl variant coformers in IV and V and the dihydroxyl variant coformer in I showed similar crystal packing because both these coformers have hydroxyl positions fixed at 1,3-positions of the aromatic ring which facilitated O–H···N bond with piperazine and O–H···O bond with amide carbonyl for helix propagation. The extra hydroxyl group is utilized for an intramolecular hydrogen bonding in cocrystal IV and an intermolecular hydrogen bonding with water in cocrystal V across the layers without disrupting the isostructurality. Cocrystal II contains amide N–H···O dimer and O–H···N hydrogen bond with the piperazine, but is unable to form O–H···O hydrogen bond for helical networking. Nevertheless, II maintains isostructurality with the cocrystals I, IV and V because of its ability to form similar 2D layer and interlayer stabilization through C–H···O, C–H···π, O–H···N and Cl···O contacts. Surprisingly, the hydroquinone cocrystal III results in a totally different crystal structure (Fig.9) from a twisted aripiprazole conformation. Whereas in all other cocrystals, an extended conformation of aripiprazole is seen. The layer propagation in III is found to be different from layers observed in other four structures.

The spectral shifts of carbonyl group in cocrystals I-V correlate well with the intermolecular contacts noticed in the crystal structures and their relative strengths. The carbonyl oxygen participates in three types of interactions in I, IV and V (N–H···O, O–H···O, Cl···O) whereas only two types of contacts are seen in III (N–H···O, O–H···O) and II (N–H···O, Cl···O). Due to this, there are relatively larger carbonyl frequency shifts in the higher melting cocrystals I, IV and V (1652 cm^{-1}) compared to lower melting cocrystals III (1662 cm^{-1}) and II (1673 cm^{-1}). Hirshfeld surface maps are used for a graphical representation of number of intermolecular contacts formed by aripiprazole in various cocrystals by red color hot spots on the surfaces (Fig.11).

Structure-property correlation

When we try to correlate the crystal packing features with the observed melting points, the cocrystal structures I, IV and V with strong helical networks are identified as high melting solids (170-180°C). On the other hand, cocrystals II and III which lack helical networks and sustained by softer interactions between the layers are identified as low melting solids (120-140°C). Two important conclusions can be inferred from the present study. First, aripiprazole cocrystals are higher melting compared to its parent drug because the unutilized piperazine N acceptor in single component system was utilized for hydrogen

bonding in multi-component cocrystal. Second, for structure to be more stable, the strong hydrogen bonds must be spread across the three dimensional space/all three directions. Cocrystal I is sustained by the propagation of conventional hydrogen bonds, N–H···O, O–H···N and O–H···O, in all directions whereas cocrystal II contains N–H···O, O–H···N but lacks O–H···O hydrogen bond and accordingly melts at lower temperature. In cocrystal III, all three hydrogen bonds as noticed in cocrystal I are seen; despite this the structure is low melting. This is because all three strong hydrogen bonds have been utilized only for the construction of a discrete unit (Fig.9a) leaving its two and three dimensional crystal packing essentially governed by weaker C–H···O, C–H···π and C–H···Cl contacts. Such contacts are softer and can be easily broken. Further, the conformation of aripiprazole in cocrystal III is twisted and higher in energy[9c-d] compared to the stable extended conformation in cocrystal I. Thus our study attempts to provide a detailed understanding about the role of coformer and aripiprazole having a direct influence on the crystal packing and thermal stability. The presence/absence of hydrogen bonding along three dimensional space in crystals is shown to be an important factor for structural stability and the melting point variations.

Conclusions

The strong phenol-piperazine O–H···N hydrogen bonding was utilized for designing five novel cocrystals of aripiprazole drug with aromatic hydroxyl coformers. Cocrystals were obtained by solid state grinding approach and by crystallization route and were conformed to be new phases by Powder X-ray diffraction and Infrared spectroscopy. Interestingly, the melting points in cocrystals were altered significantly, although the coformers were similar in size and adopted isostructural packing in four of them. Single crystal X-ray diffraction was carried out to gain deeper insights on the molecular packing and intermolecular contacts. The melting point variations in the cocrystals were attributed to the molecular arrangements in the crystal with intermolecular hydrogen bonds serving to constrain the motion of the molecules and stabilize them in the solid state. Especially, the molecular shape of the coformer was found to play a crucial role in facilitating O–H···O hydrogen bonding between hydroxyl and amide carbonyl and lead to three dimensional helix formation. The coformers with hydroxyls at 1,3-position on the aromatic ring were able to form the helical networks, whereas coformers with hydroxyls at 1,2 or 1,4-positions were able not form similar helices, and only weaker interlayer contacts are seen in these crystals which make them as lower melting solids. The well accepted notion that the melting points in the cocrystals correlate well with the melting points of coformers is violated here, and the possible reasons are attributed to the spread of strong hydrogen bonds across the three dimensional space providing a greater structural stability in higher melting cocrystals.

Acknowledgements

We acknowledge the CSIR, New Delhi, for financial support as a part of XII five-year plan program under the titles AARF (CSC0406) and ORIGIN (CSC0108). JBN thank SERB, India for start-up grant and fellowship (No.SB/FT/CS-128/2014). Mr. Sivanarayan from centre for X-ray crystallography is thanked for his support on PXRD data. Dr. Sistla Ramakrishna and Mr. Mayank Singh of CSIR-IICT and Dr. Suryanarayan Cherukuvada of IISC, Bangalore are thanked for DSC and TGA scans. We also take this opportunity to thank Mr. Ramkumar from Polymer Division, Ms. Monika Garg and Ms. Vinusha Pendota for their timely help. The director Dr. Srivari Chandrasekhar is thanked for his motivation and encouragement.

References

1) (a) A. R. Katritzky, R. Jain, A. Lomaka, R. Petrukhin, U. Maran and M. Karelson, *Cryst. Growth Des.*, 2001, **1**, 261–265; (b) A. D. Bond, *New J. Chem.*, 2004, **28**, 104–114.; (c) V. R. Thalladi, M. Nüsse and R. Boese, *J. Am. Chem. Soc.*, 2000, **122**, 9227–9236; (d) V. R. Vangala, B. R. Bhogala, A. Dey, G. R. Desiraju, C. K. Broder, P. S. Smith, R. Mondal, J. a K. Howard and C. C. Wilson, *J. Am. Chem. Soc.*, 2003, **125**, 14495–14509.
2) (a)E. Nauha, E. Kolehmainen and M. Nissinen, *CrystEngComm*, 2011, **13**, 6531; (b) George, J. Forrest, P. E. Bonnett and P. T. Gavin. U.S. Patent 8318789, issued November 27, 2012; (c) T. Chiodo, E. Klimov, A. Schaefer, H. W. Hoeffken, R. Hellman, A. Kabat, R. Israels, G. Schnabel, M. Bratz, C. Kibat and W. Houy, U.S. Patent Application 14388462, filed March 20, 2013; (d) J. Pernak, J. Shamshina, P. Tadeusz, A. Syguda, D. Janiszewska, M. Smiglak, G. Gurau, D. T. Daly and R. D. Rogers. U.S. Patent Application 13808790, filed July 6, 2011.
3) (a) A. S. Cannon and J. C. Warner, *Cryst. Growth Des.*, 2002, **2**, 255–257; (b) E. Stoler and J. C. Warner, *Molecules*, 2015, **20**, 14833–48.
4) S. Aitipamula, R. Banerjee, A. K. Bansal, K. Biradha, M. L. Cheney, A. R. Choudhury, G. R. Desiraju, A. G. Dikundwar, R. Dubey, N. Duggirala, P. P. Ghogale, S. Ghosh, P. K. Goswami, N. R. Goud, R. R. K. R. Jetti, P. Karpinski, P. Kaushik, D. Kumar, V. Kumar, B. Moulton, A. Mukherjee, G. Mukherjee, A. S. Myerson, V. Puri, A. Ramanan, T. Rajamannar, C. M. Reddy, N. Rodriguez-Hornedo, R. D. Rogers, T. N. G. Row, P. Sanphui, N. Shan, G. Shete, A. Singh, C. C. Sun, J. A. Swift, R. Thaimattam, T. S. Thakur, R. Kumar Thaper, S. P. Thomas, S. Tothadi, V. R. Vangala, N. Variankaval, P. Vishweshwar, D. R. Weyna, and M. J. Zaworotko, *Cryst. Growth Des.*, 2012, **12**, 2147–2152
5) (a) S. L. Childs, G. P. Stahly and A. Park, *Mol. Pharm.*, 2007, **4**, 323–38; (b) N. J. Babu, L. S. Reddy and A. Nangia, *Mol. Pharm.*, 2007, **4**, 417–434; (c) C. B. Aakeröy, A. M. Beatty and B. A. Helfrich, *J. Am. Chem. Soc.*, 2002, **124**, 14425–14432.
6) P. Vishweshwar, J. A. McMahon, J. A. Bis and M. J. Zaworotko, *J. Pharm. Sci.*, 2006, **95**, 499–516.
7) (a) W. Jones, W. D. S. Motherwell and A. V. Trask, *MRS Bull.*, 2011, **31**, 875–879. (b) R. Thakuria, A. Delori, W. Jones, M. P. Lipert, L. Roy and N. Rodríguez-Hornedo, *Int. J. Pharm.*, 2013, **453**, 101–25; (c) J. W. Steed, *Trends Pharmacol. Sci.*, 2013, **34**, 185–93; (d) D. J. Good and N. Rodríguez-Hornedo, *Cryst. Growth Des.*, 2009, **9**, 2252–2264; (e) N. J. Babu and A. Nangia, *Cryst. Growth Des.*, 2011, **11**, 2662–2679; (f) N. J. Babu, P. Sanphui and A. Nangia, *Chem. - An Asian J.*, 2012, **7**, 2274–2285; (g) H. G. Brittain, *J. Pharm. Sci.*, 2013, **102**, 311–7; (h) S. Chattoraj, L. Shi, C. C. Sun, *CrystEngComm*, 2010, **12**, 2466-2472; (i) N. Blagden, S. J. Coles, and D. J. Berry, *CrystEngComm*, 2014, **16**, 5753-5761.
8) (a) N. Schultheiss and A. Newman, *Cryst. Growth Des.*, 2009, **9**, 2950–2967; (b) P. Vishweshwar, A. Nangia and V. Lynch, *Cryst. Growth Des.,* 2003, **3**, 783-790; (c) R. D. Bailey Walsh, M. W. Bradner, S. Fleischman, L. A. Morales, B. Moulton, N. Rodriguez-Horedo and M. J. Zaworotko, *Chem. Commun.,* 2003, 186-187. (d) J. T. Wu, J. G. Zhang, T. Li, Z. M. Li and T. L. Zhang, *RSC Adv.,* 2015, **5**, 28354-28359; (e) C. B. Aakeröy, S. Forbes and J. Desper, *J. Am. Chem. Soc.* 2009, **131**, 17048-17049; (f) S. Basavoju, D. Bostrom and S. P. Velaga, Pharmacol. Res., 2008, 25, 530–540; (g) L. J. Thompson, R. S. Voguri, L. Male, M. Tremayne, *CrystEngComm*, 2011, **13**, 4188-4195; (h) D. P. McNamara, S. L. Childs, J. Giordano, A. Iarriccio, J. Cassidy, M. S. Shet, R. Mannion, E. O'Donnell and A. Park, *Pharm. Res.*, 2006, **23**, 1888-1897; (i) A. D. Bond, *CrystEngComm*, 2006, 8, 333-337; (j) D. Braga, E. Dichiarante, G. Palladino, F. Grepioni, M. R. Chierotti, R. Gobetto, and L.

Pelleogrino, CrystEngComm, 2010, 12, 3534-3536; (k) K. Bica, J. Shamshina, W. L. Hough, D. R. MacFarlane, R. D. Rogers, CrystEngComm, 2011, 47, 2267-2269.

9) L. Tessler and I. Goldberg, *J. Incl. Phenom. Macrocycl. Chem.*, 2006, **55**, 255–261; (b) D. E. Braun, T. Gelbrich, V. Kahlenberg, R. Tessadri, J. Wieser and U. J. Griesser, *J. Pharm. Sci.*, 2009, **98**, 2010–26; (c) J. B. Nanubolu, B. Sridhar, K. Ravikumar and S. Cherukuvada, *CrystEngComm*, 2013, **15**, 4321; (d) S. P. Delaney, D. Pan, S. X. Yin, T. M. Smith and T. M. Korter, *Cryst. Growth Des.*, 2013, **13**, 2943–2952; (e) S. P. Delaney, T. M. Smith, D. Pan, S. X. Yin and T. M. Korter, *Cryst. Growth Des.*, 2014, **14**, 5004–5010.

10) (a) J. B. Nanubolu, B. Sridhar, V. S. P. Babu, B. Jagadeesh and K. Ravikumar, *CrystEngComm*, 2012, **14**, 4677; (b) E. Freire, G. Polla and R. Baggio, *Acta Crystallogr. C.*, 2012, **68**, o170–3; (c) E. Freire, G. Polla and R. Baggio, *Acta Crystallogr. C.*, 2012, **68**, o235–9; (d) E. Freire, G. Polla and R. Baggio, *Acta Crystallogr. C.*, 2013, **69**, 186–90; (e) E. Freire, G. Polla and R. Baggio, *J. Mol. Struct.*, 2014, **1068**, 43–52.

11) Cambridge Structural Database, ver. 5.36. ConQuest 1.17, November 2014 release, May 2015 update, CCDC, Accessed at: www.ccdc.cam.ac.uk

12) (a) Bruker (2008). *DIFFRAC* EVA, http://www.bruker-axs.com/eva.html; (b) PowDLL: A program for the interconversion of powder diffraction data files, N.Kourkoumelis, University of Ioannina, Greece, 2014, Accessed at: http://users.uoi.gr/nkourkou/powdll/ (c) C. F. Macrae, I. J. Bruno, J. A. Chisholm, P. R. Edgington, P. McCabe, E. Pidcock, L. Rodriguez-Monge, R. Taylor, J. van de Streek and P. A. Wood, *J. Appl. Crystallogr.*, 2008, 41, 466–470; (d) P. J. Turner, XMGRACE, Version 5.1. 19. Center for Coastal and Land-Margin Research, Oregon Graduate Institute of Science and Technology, Beaverton, OR (2005), Accessed at: http://plasma-gate.weizmann.ac.il/Grace/ (e) LabSpec software 5.54.15 by Horiba Jobin Vyon, 2008, Accessed at: http://www.horiba.com/scientific/products/raman-spectroscopy/software/functionality/

13) W. M. Haynes, CRC Handbook of Chemistry and Physics, Taylor & Francis, 95th edn, 2014.

14) (a) Bruker, SAINT and SMART, Bruker AXS Inc., Madison, Wisconsin, USA, 2001; (b) G. M. Sheldrick, *Acta Crystallogr., Sect. A: Found. Crystallogr.*, 2008, **64**, 112–122. (c) G. M. Sheldrick, SHELXL 2014/7, University of Göttingen, Germany, 2014; (d) A. Spek, *J. Appl. Crystallogr.*, 2003, **36**, 7–13; (e) L. J. Barbour, *Supramol. Chem.,* 2001, **1**, 189–191; (f) L. J. Barbour, X-Seed, Graphical Interface to SHELX-97 and POV-Ray; University of Missouri-Columbia, Columbus, MO, 1999.

15) (a) S. K. Wolff, D. J. Grimwood, J. J. McKinnon, D. Jayatilaka and M. A. Spackman, CrystalExplorer 2.1, University of Western Australia, Perth, 2007; (b) M. A. Spackman and D. Jayatilaka, *CrystEngComm*, 2009, **11**, 19-32. (c) J. J. Mckinnon, D. Jayatilaka and M. A. Spackman, *Chem. Commun.*, 2007, 3814-3816.

16) A. J. Cruz-Cabeza, *CrystEngComm*, 2012, **14**, 6362–6365

17) (a) D. L. Pavia, G. M. Lampman, G. S. Kriz, J. R. Vyvyan, Introduction to Spectroscopy, 4th Ed. 2009, Brooks/Cole, Belmont, USA; (b) R. M. Silverstein, F. X. Webster, D. J. Kiemle, Spectrometric Identification of Organic Compounds, 7th Ed. 2005, John Wiley & Sons Inc, USA.

18) (a) U.S. Food and Drug Administration, Center for Food Safety and Applied Nutrition. 2011. "EAFUS: A food additive database". Accessed at: http://www.fda.gov/Food/IngredientsPackagingLabeling/ucm115326.htm; (b) Food and Drug Administration, FDA Select Committee on GRAS Substances (SCOGS) Database Overview, 2013, Accessed at: http://www.fda.gov/food/ingredientspackaginglabeling/gras/scogs/ucm2006852.htmN.

19) (a) A. R. Voth, P. Khuu, K. Oishi and P. S. Ho, Nat. Chem. 2009, 1, 74-79; (b) J. P. M. Lommerse, A. J. Stone, R. Taylor and F. H. Allen, *J. Am. Chem. Soc.* 1996, **118**, 3108-3116.

Table 1. Crystal data of five aripiprazole cocrystals.

Compound reference	Cocrystal I	Cocrystal II	Cocrystal III	Cocrystal IV	Cocrystal V
Chemical formula	$C_{23}H_{27}Cl_2N_3O_2$•$C_6H_6O_2$	$C_{23}H_{27}Cl_2N_3O_2$ •$C_6H_6O_2$•0.293H_2O	$C_{23}H_{27}Cl_2N_3O_2$•$C_6H_6O_2$	$C_{23}H_{27}Cl_2N_3O_2$ •$C_6H_6O_3$•0.256H_2O	$C_{23}H_{27}Cl_2N_3O_2$•$C_6H_6O_3$•H_2O
Formula Mass	558.48	563.17	558.48	578.58	590.48
Crystal system	Monoclinic	Monoclinic	Triclinic	Monoclinic	Monoclinic
a/Å	14.7282(12)	14.7513(16)	6.9061(8)	14.7016(11)	14.8405(6)
b/Å	9.8820(8)	9.9206(11)	9.4544(11)	9.9378(7)	10.2671(4)
c/Å	20.8815(14)	20.9131(17)	22.484(3)	20.9827(12)	20.6587(9)
α/°	90	90	96.056(2)	90	90
β/°	111.174(5)	111.104(6)	95.355(2)	111.121(4)	110.2190(10)
γ/°	90	90	100.696(2)	90	90
Unit cell volume/$Å^3$	2834.0(4)	2855.2(5)	1424.9(3)	2859.7(3)	2953.8(2)
Temperature/K	293(2)	293(2)	293(2)	293(2)	293(2)
Space group	*P*21/*c*	*P*21/*c*	*P*$\bar{1}$	*P*21/*c*	*P*21/*c*
No. of formula units per unit cell, *Z*	4	4	2	4	4
Radiation type	MoKα	MoKα	MoKα	MoKα	MoKα
Absorption coefficient, μ/mm^{-1}	0.268	0.267	0.267	0.271	0.266
2θ Min-Max /°	4.2, 51.4	4.2, 50.0	3.6, 51.4	4.2, 51.4	4.2, 50.0
No. of reflections measured	28020	26716	14353	26964	27780
No. of independent reflections	5359	5044	5395	5420	5225
R_{int}	0.0213	0.0286	0.0278	0.0189	0.0248
Final R_1 values ($I > 2\sigma(I)$)	0.0363	0.0648	0.0493	0.0335	0.0730
Final $wR(F^2)$ values ($I > 2\sigma(I)$)	0.1021	0.1560	0.1177	0.0935	0.2054
Final R_1 values (all data)	0.0421	0.0781	0.0827	0.0375	0.0824
Final $wR(F^2)$ values (all data)	0.1075	0.1647	0.1348	0.0977	0.2151
Goodness of fit on F^2	1.026	1.124	1.016	1.030	1.080
Min. and Max. Resd. Den. e/ $Å^3$	-0.18, 0.40	-0.25, 0.50	-0.21, 0.40	-0.19, 0.22	-0.29, 0.85
CCDC number	**1430981**	**1430982**	**1430983**	**1430984**	**1430980**

Table 2. Prominent hydogen bonding and non-covalent interactions in five cocrystal structures.

Cocrystal	**D–H···A**	**D–H /Å**	**H···A /Å**	**D···A /Å**	**D–H···A /°**
I	O3–H3O···N2	0.82	1.97	2.757(2)	163
	O4–H4O···O1^{i}	0.89	1.88	2.765(2)	172

	N1–H1N···O1[il]	0.80	2.13	2.930(2)	172
	C8–H8···O3[iii]	0.93	2.65	3.454(2)	145
	C16–H16···O4[iii]	0.97	2.61	3.548(2)	162
	C22–H22···Cl1[iv]	0.93	2.92	3.790(2)	156
	C14–H14B···Cg1[v]	0.97	2.98	3.522(2)	117
	C17–H17A···Cl1	0.97	2.61	3.218(2)	121
	Cl1···O1[vi]			2.962(1)	

[i] 2-x,1/2+y,3/2-z; [ii] 2-x,-y,1-z; [iii] 1-x,-1/2+y,3/2-z; [iv] -x,1/2+y,3/2-z; [v] 1-x,1/2+y,3/2-z; [vi] 1-x, -y, 1-z; Cg1 is the centroid of C24-C29 atoms.

II	O3–H3O···N2	0.82	1.97	2.756(4)	159
	O4–H4O···O3	0.82	2.27	2.680(7)	111
	O4–H4O···O5W	0.82	2.33	3.139(2)	169
	N1–H1N···O1[i]	0.81	2.09	2.901(3)	174
	C8–H8···O3[ii]	0.93	2.80	3.589(5)	144
	C8–H8···O4[ii]	0.93	2.78	3.451(7)	130
	C22–H22···Cl1[iii]	0.93	2.95	3.825(4)	157
	C14–H14B···Cg1[iv]	0.97	2.95	3.542(4)	120
	C17–H17A···Cl1	0.97	2.60	3.212(3)	121
	O3···O5W			2.415(2)	
	O5W···Cl2[v]			3.269(1)	
	Cl1···O1[vi]			2.952(2)	

[i] -x,-y,1-z; [ii] 1-x,-1/2+y,1/2-z; [iii] 2-x,1/2+y,1/2-z; [iv] 1-x,1/2+y,1/2-z; [v] 2-x,-1/2+y,1/2-z; [vi] 1-x, -y, 1-z; Cg1 is the centroid of C24-C29 atoms.

III	O3–H3O···N2	0.83	1.99	2.803(3)	166
	O4–H4O···O1[i]	0.81	1.95	2.754(3)	175
	N1–H1N···O1[i]	0.81	2.22	2.952(3)	151
	C28–H28···O1[i]	0.93	2.70	3.364(4)	129
	C2–H2A···O2[ii]	0.97	2.52	3.422(4)	155
	C17–H17A···Cl1[ii]	0.97	2.93	3.704(3)	137
	C3–H3B···Cg1[iii]	0.97	2.89	3.849(3)	171
	C15–H15B···Cl1	0.97	2.74	3.286(3)	116

[i] 3-x,1-y,2-z; [ii] 1+x,y,z; [iii] 3-x,2-y,2-z; Cg1 is the centroid of C4-C9 atoms.

IV	O3–H3O···N2	0.85	1.93	2.739(2)	159
	O5–H5O···O1[i]	0.88	1.85	2.720(2)	173
	O3–H3O···O4	0.85	2.41	2.766(2)	106
	O4–H4O···O5	0.89	2.19	2.683(2)	115
	O4–H4O···O6W	0.89	1.75	2.539(6)	147
	N1–H1N···O1[ii]	0.82	2.10	2.916(2)	173
	C8–H8···O3[iii]	0.93	2.73	3.541(2)	146
	C16–H16A···O5[iii]	0.97	2.56	3.506(2)	165
	C8–H8···Cg2[iiii]	0.93	2.78	3.689(2)	166
	C14–H14B···Cg1[iv]	0.97	2.94	3.534(2)	121
	C22–H22···Cl1[v]	0.93	2.94	3.813(2)	157
	C17–H17A···Cl1	0.97	2.60	3.204(2)	120
	C13–H13A···O4	0.97	2.60	3.126(2)	114

	O6W···Cl2[vi]			3.258(6)	
	O6W···O3[iv]			2.433(6)	
	Cl1···O1[vi]			2.965(1)	

[i] -1-x,1/2+y,1/2-z; [ii] -1-x,1-y,1-z; [iii] -x,-1/2+y,1/2-z; [iv] -x,1/2+y,1/2-z; [v] 1-x,1/2+y,1/2-z; [vi] -1+x,y,z; [vi] –x, 1-y, 1-z; Cg1 is centroid of C24-C29 atoms and Cg2 is centroid of C24/C29.

V	O3–H3O···N2	0.82	1.78	2.545(7)	154
	O5–H5O···O1[i]	0.98	1.83	2.797(6)	174
	O4–H4O···O6W	0.98	2.68	3.501(9)	141
	N1–H1N···O1[ii]	0.83	2.09	2.917(4)	171
	C8–H8···O3[iii]	0.93	2.76	3.597(7)	150
	C17–H17B···O4[iii]	0.97	2.65	3.275(7)	122
	C16–H16A···Cg2[iii]	0.97	2.74	3.652(7)	157
	C14–H14B···Cg1[iv]	0.97	2.83	3.570(7)	134
	C22–H22···Cl1[v]	0.93	2.91	3.812(5)	165
	C27–H27···O1[i]	0.93	2.63	3.280(2)	127
	C3–H3A···Cg3 [vi]	0.97	2.80	3.699(5)	155
	C17–H17A···Cl1	0.97	2.63	3.220(4)	119
	Cl1···O1[vii]			2.987(3)	

[i] -x,1/2+y,1/2-z; [ii] -x,-y,1-z; [iii] 1-x,-1/2+y,1/2-z; [iv] 1-x,1/2+y,1/2-z; [v] 2-x,1/2+y,1/2-z; vi -1+x, -1+y, z; [vii] 1-x, -y, 1-z; Cg1 is the centroid of C28/C29 atoms; Cg2 is of C26/C27 atoms; Cg3 is of C18-C23 atoms.

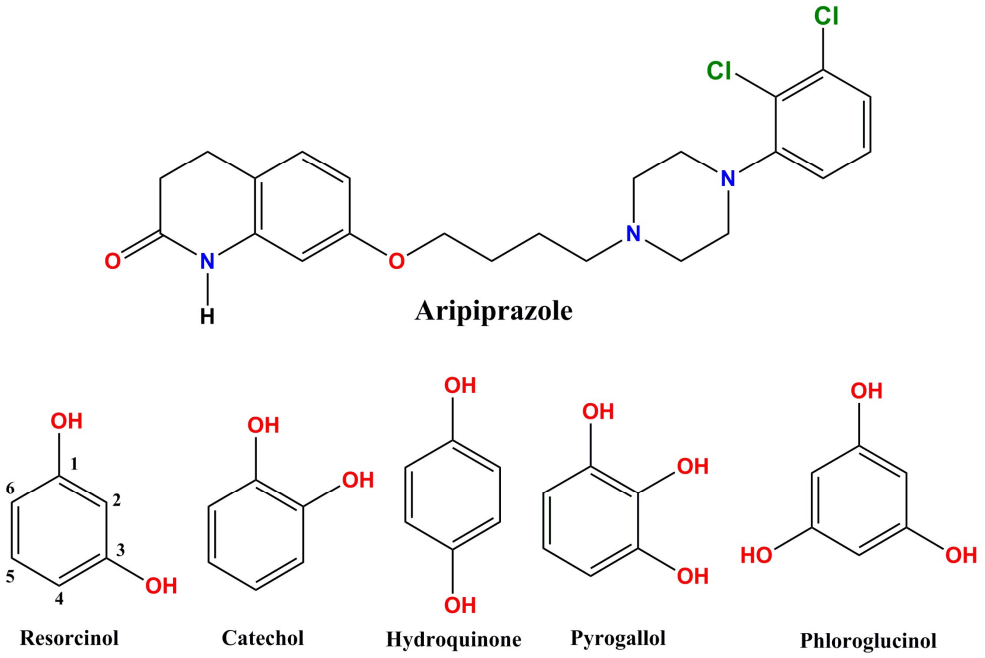

Scheme 1. Molecular structures of the aripiprazole drug and five coformers used in co-crystallization experiments. The hydroxyl positions on the aromatic ring are indicated by carbon atom labels.

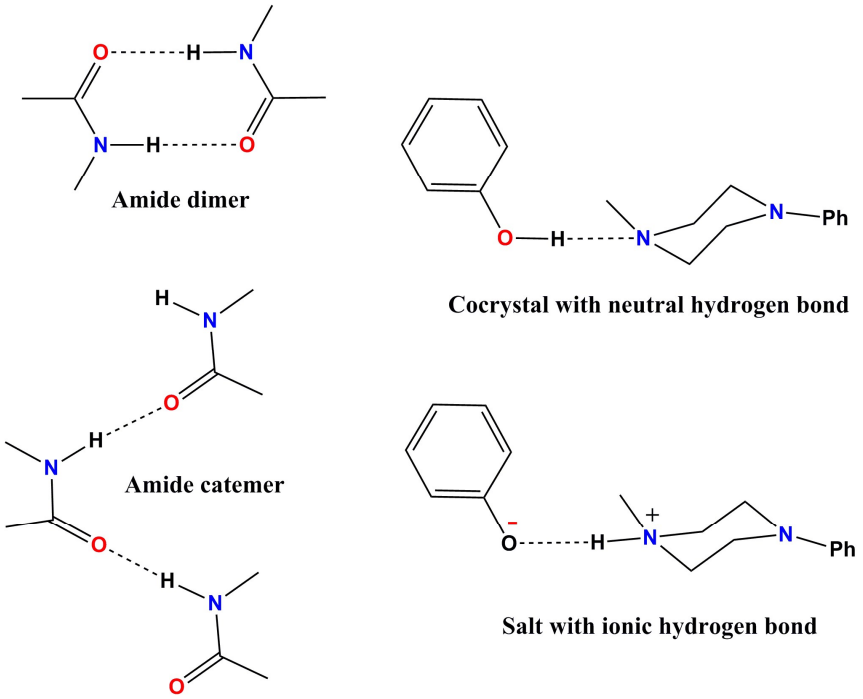

Scheme 2. Schematic representation of hydrogen bond motifs formed by amide functional group as N–H···O dimer and catemer (left side) and phenol and piperazine interactions as neutral O–H···N and ionic N^{+}–H···O^{-} interactions (right side)

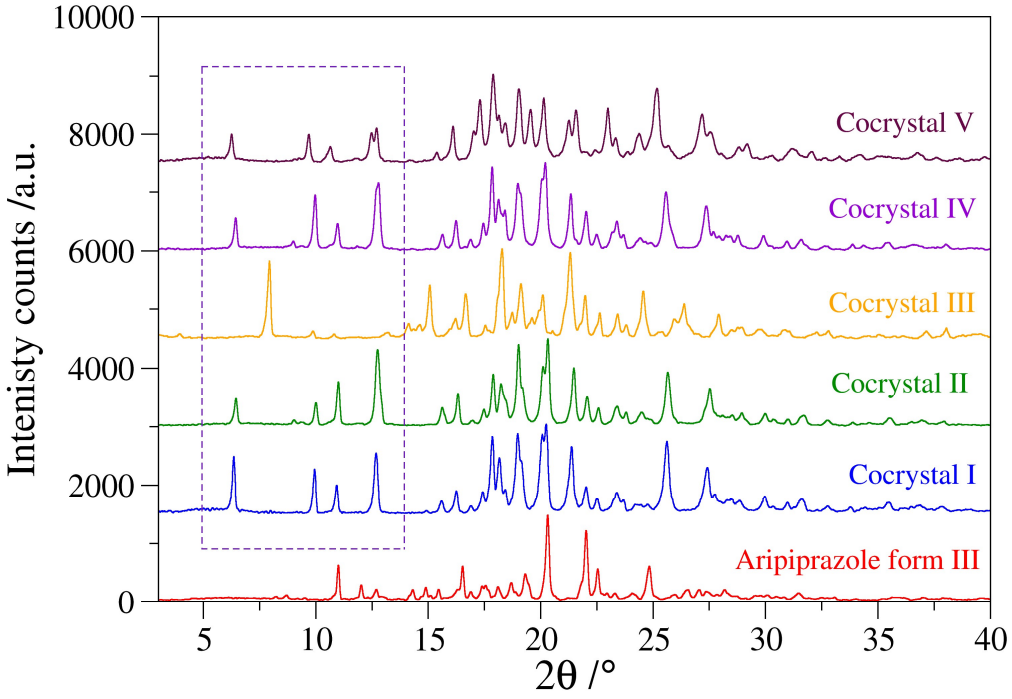

Fig. 1. Comparison of experimental powder XRD patterns of aripiprazole with newly formed cocrystal phases. Distinct peaks are seen in the cocrystal phases. Cocrystal I, II, IV and V showed some similarities in their PXRD patterns in 5-15° 2θ range suggesting them to adopt an isostructural packing. However, cocrystal III is different and can be distinguished from its characteristic peaks.

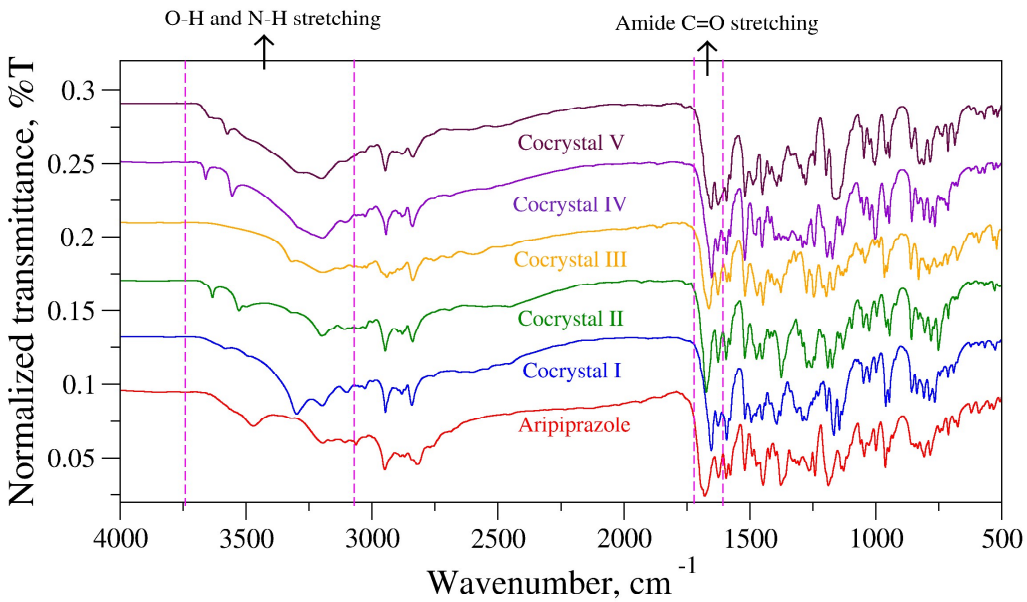

(a)

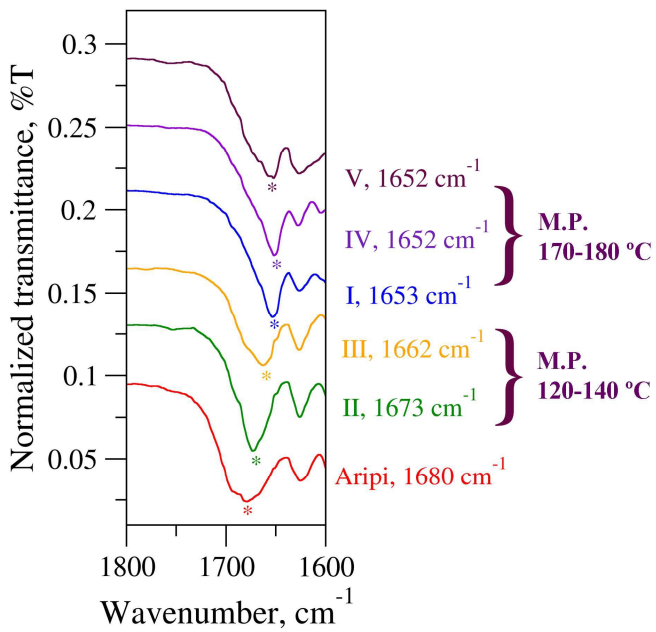

(b)

Fig. 2 (a) An overlay of FT-IR spectra of aripiprazole with five cocrystals. Important vibrational modes are labeled. (b) Region 1600-1800 cm^{-1} showing C=O stretching band shifts which correlate well with the observed M.P. of cocrystals. The larger C=O spectral shifts are indicative of stronger hydrogen bonding in higher melting point cocrystals.

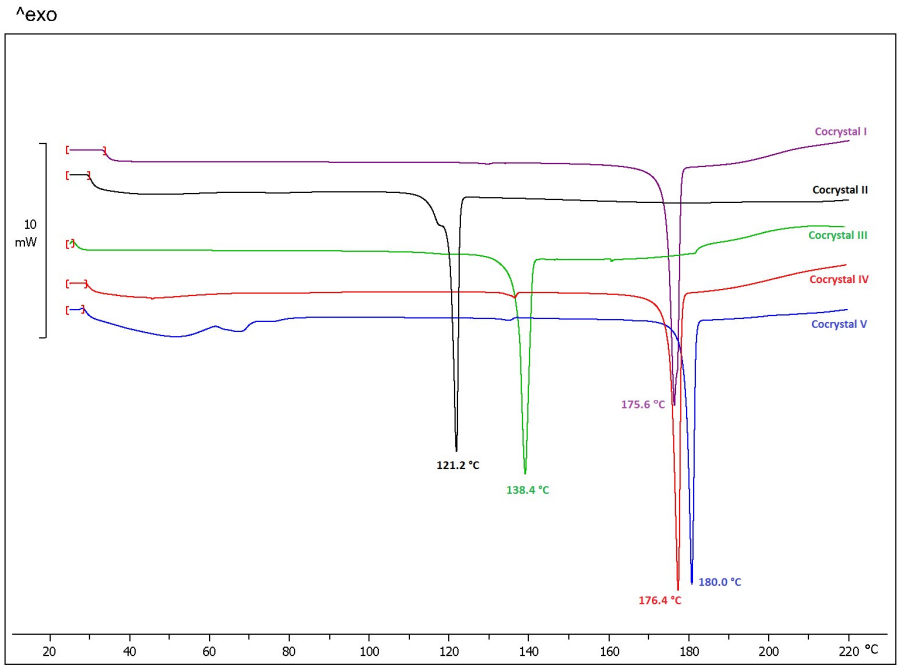

(a)

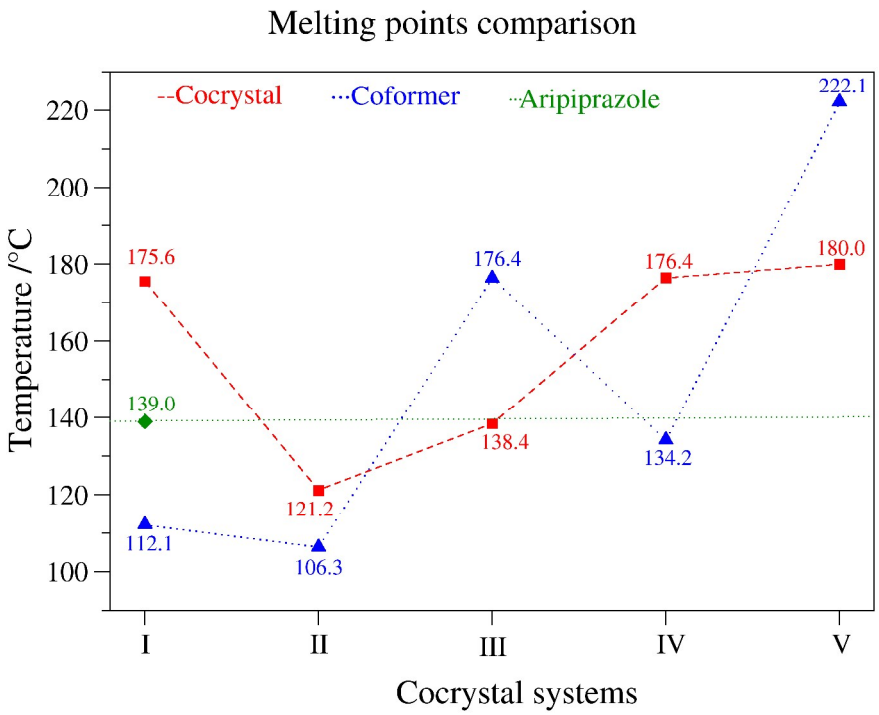

(b)

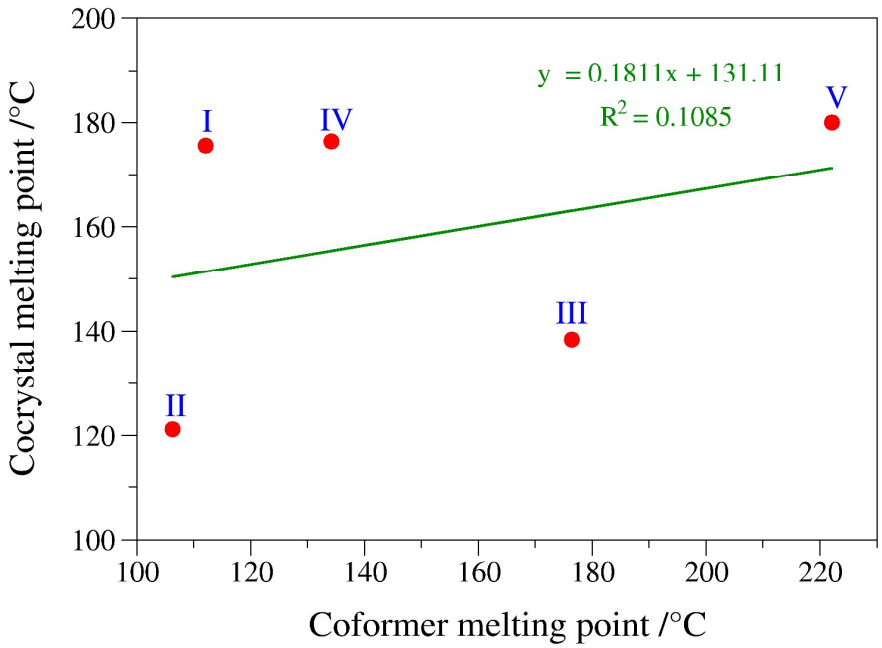

(c)

Fig. 3 (a) Differential Scanning Calorimetry (DSC) studies on cocrystal systems showing distinct melting points. (b) Comparison of melting points (M.P.) of five cocrystals with their parent compounds. Higher melting points are observed in cocrystals I and IV over their parent compounds, lower M.P. in cocrystals II and III and an intermediate M.P in cocrystal V. (c) A correlation plot between the melting points of cocrystals vs coformers.

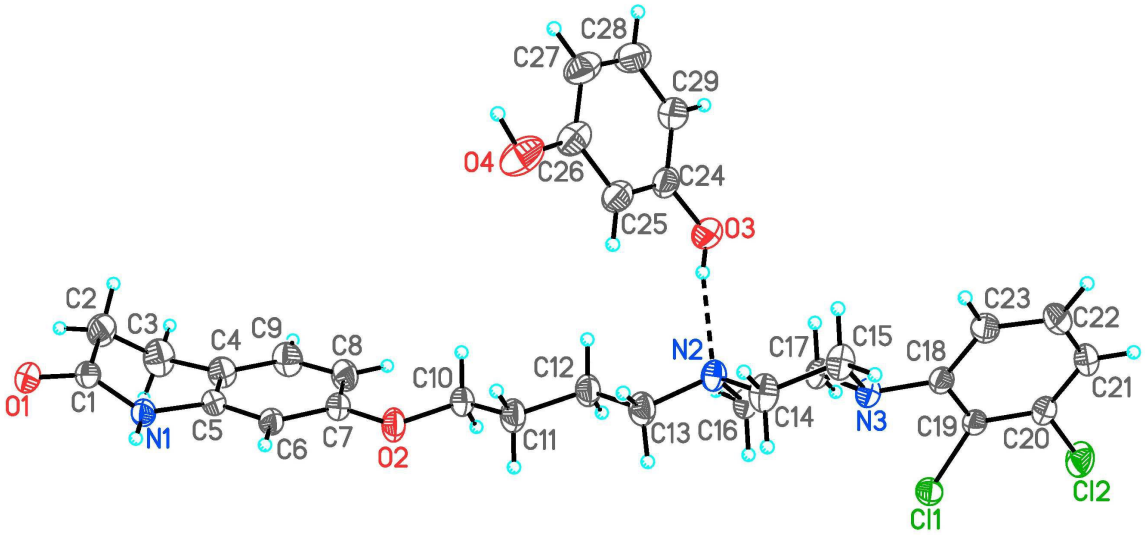

(a)

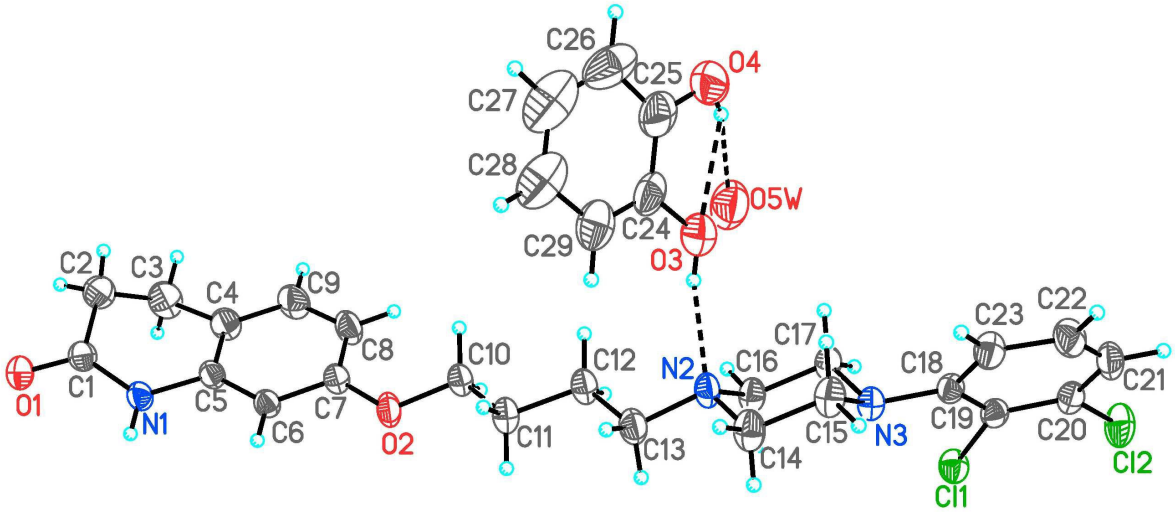

(b)

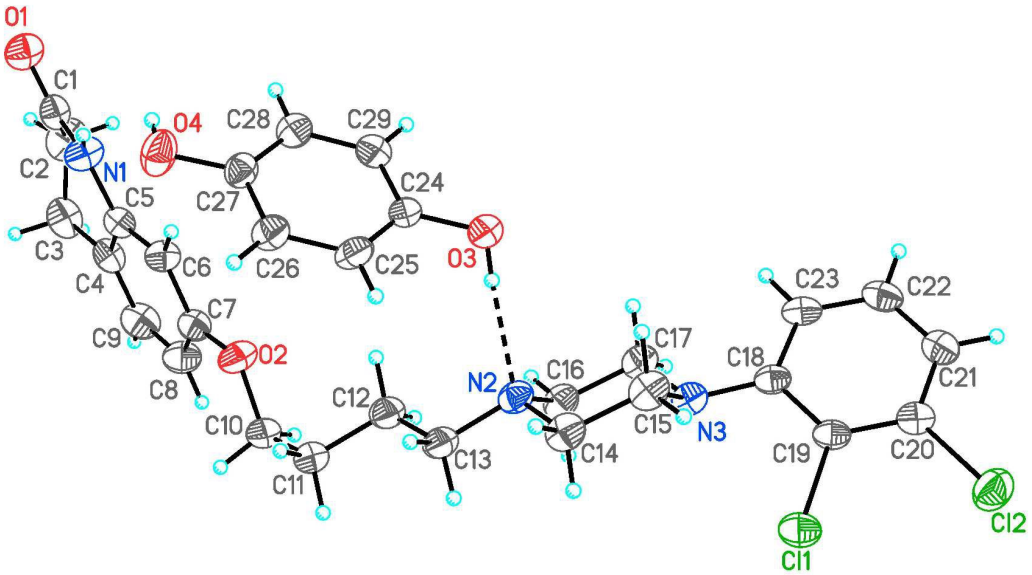

(c)

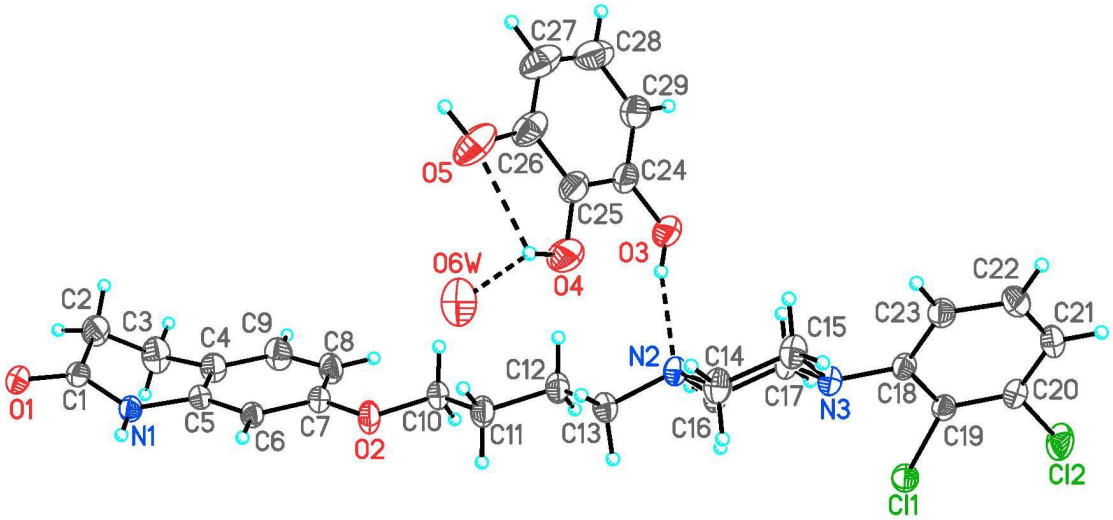

(d)

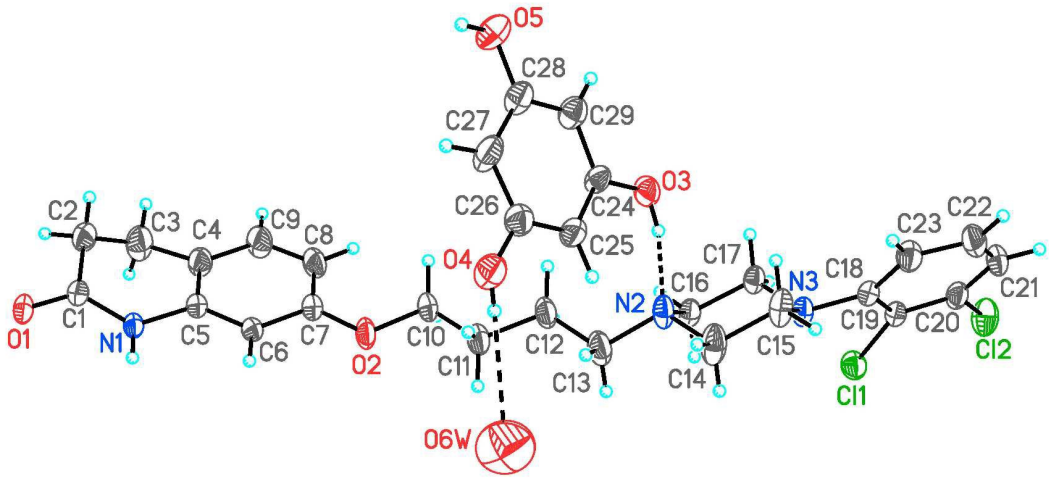

(e)

Fig. 4 ORTEP diagrams of aripiprazole cocrystals with dihydroxy and trihydroxybenzenes, with thermal ellipsoids drawn at 30% probability level (a) aripiprazole-resorcinol, I (b) aripiprazole-catechol, II (c) aripiprazole-hydroquinone, III and (d) aripiprazole-pyrogallol, IV (e) aripiprazole-phloroglucinol, V. Hydrogen atoms are shown as spheres of arbitrary radii. The stoichiometric ratio of aripiprazole to coformer is observed to be 1:1 in all structures. Cocrystals I and III are anhydrate whereas cocrystals II, IV and V are hydrated structures. Hydrogen bonding interactions are shown in dotted lines. Water protons could not be located in the difference Fourier map.

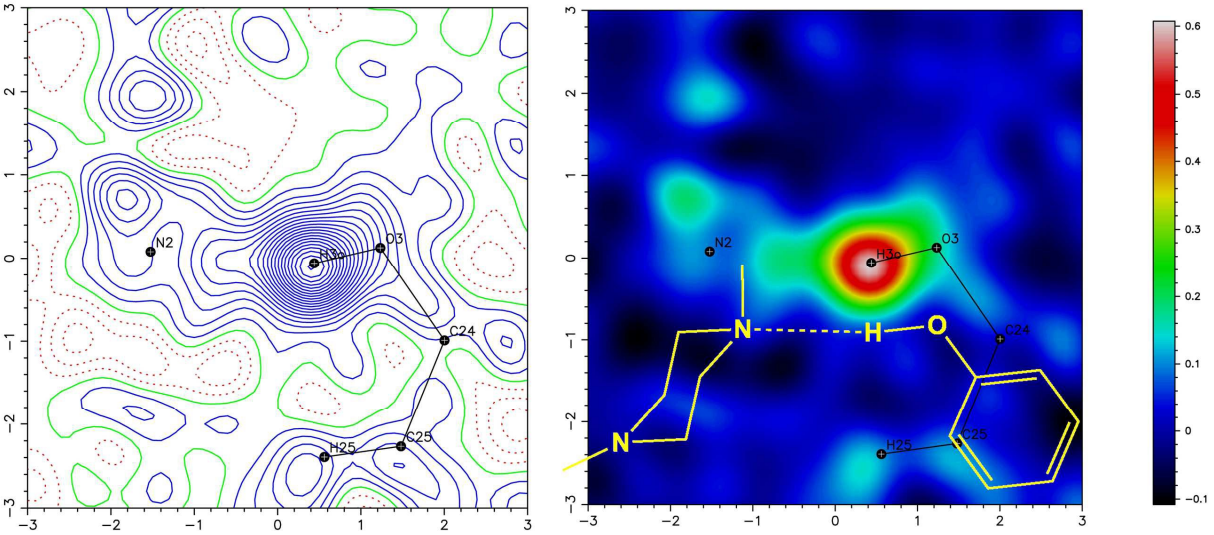

Fig. 5 A contoured difference Fourier map sliced in the plane of the phenol-piperazine bonding in cocrystal I (O3/H3O/N2 atoms), with the occupancy of atom H3O set at 0.001. The refined positions of the atoms are shown by solid circle with + mark. The contour intervals are drawn at 0.03 eÅ^3. The electron density is found maximum at O3 (2D colored map) clearly suggesting a neutral state of phenol and a neutral O–H···N hydrogen bonding with the piperazine.

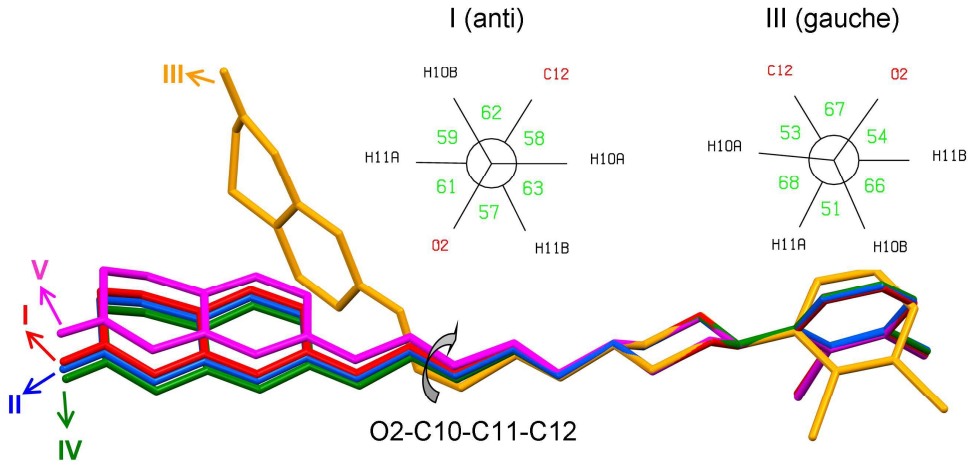

Fig. 6 Overlay of aripiprazole molecular conformations from five cocrystals. Conformations are color coded - I (red), II (blue), III (orange), IV (green) and V (magenta). Aripiprazole conformations are extended in I, II, IV and V whereas twisted in III. Overlay is made with the piperazine ring. The RMS deviation is 0.0043 for I & II, 0.0119 for I & III, 0.0059 Å for I & IV and 0.0104 Å for I & V. Newman projection plots of the torsion angle O2-C10-C11-C12 are shown to depict the *anti* orientation of O2 and C12 atoms in extended conformation while and *gauche* orientation in twisted conformation in III.

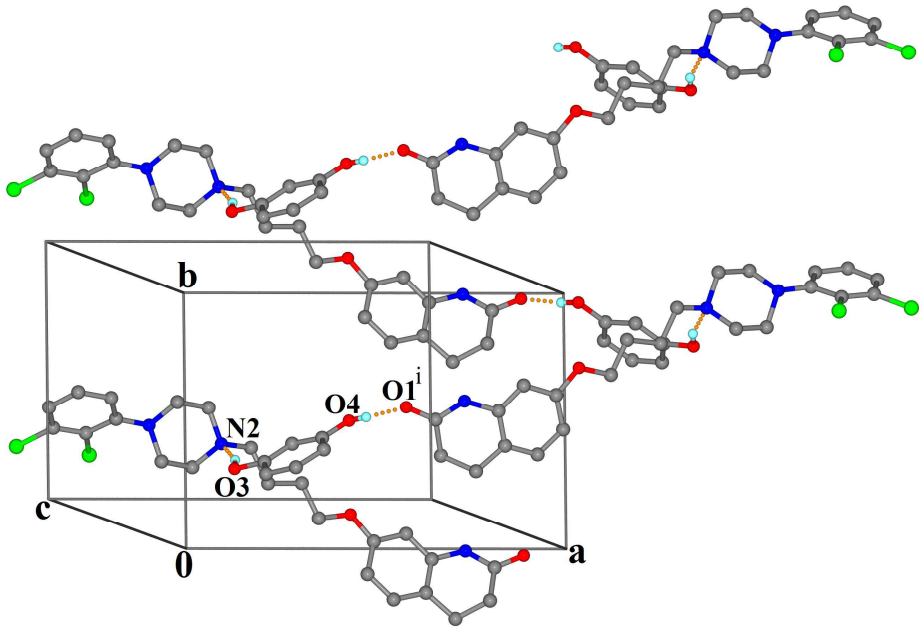

(a)

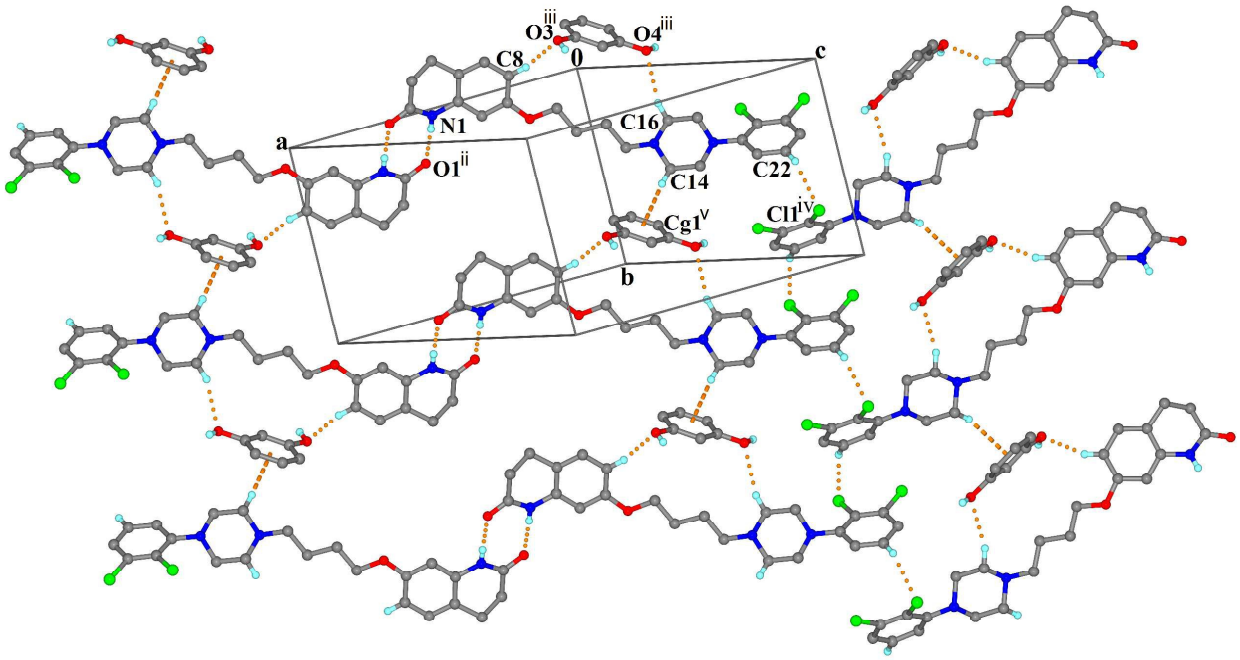

(b)

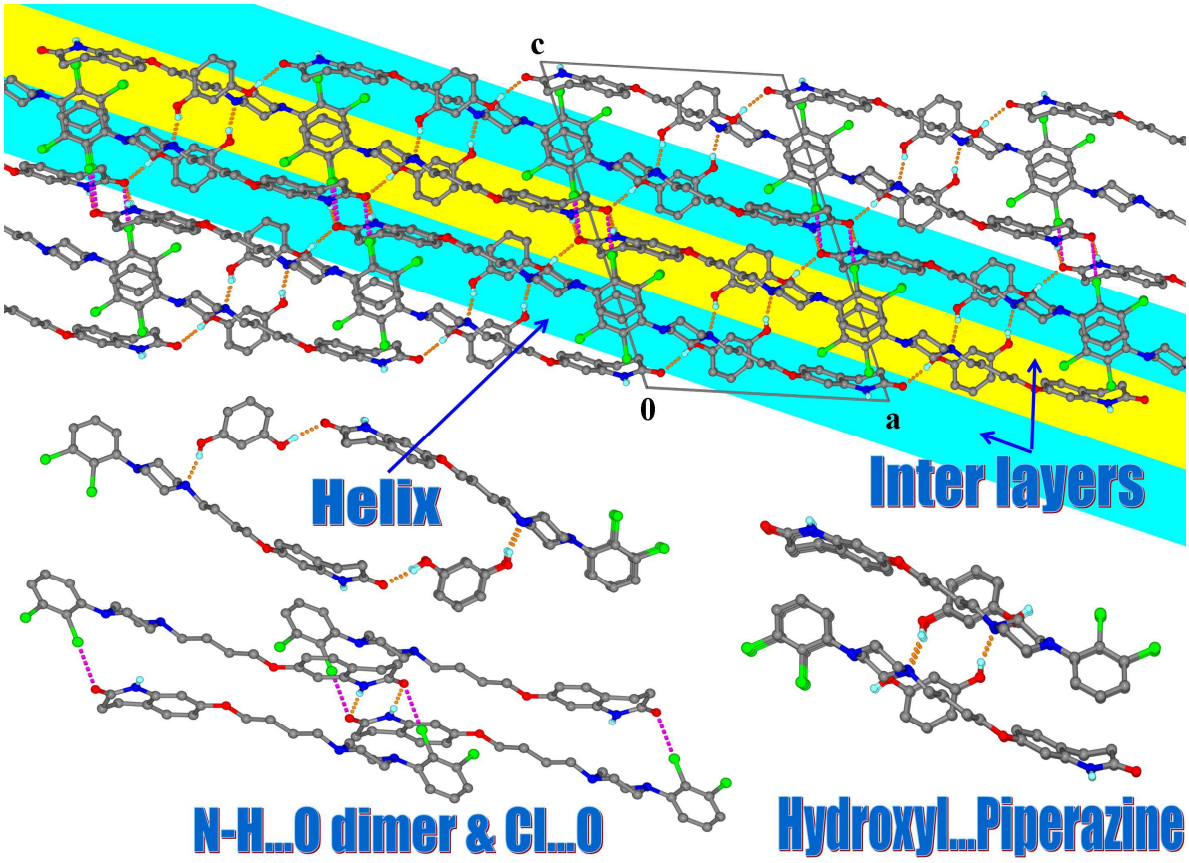

(c)

Fig. 7 (a) Helical propagation in cocrystal I through O3–H3O···N1 hydrogen bond between hydroxyl and piperazine and O4–H4O···O1 hydrogen bond between hydroxyl and amide carbonyl of aripiprazole. (b) The centrosymmetric amide N1–H1···O1 dimer is extended into a layered structure by a combination of C16–H16A···O4, C8–H8···O3, C14–H14B···Cg1 and C22–H22···Cl1 interactions. (c) Three dimensional interlayer bonding in cocrystal I. Helical networking of interlayers is highlighted. Symmetry codes, [i] 2-x,1/2+y,3/2-z; [ii] 2-x,-y,1-z; [iii] 1-x,-1/2+y,3/2-z; [iv] -x,1/2+y,3/2-z; [v] 1-x,1/2+y,3/2-z; [vi] 1-x, -y, 1-z; Cg1 is the centroid of C24-C29 atoms.

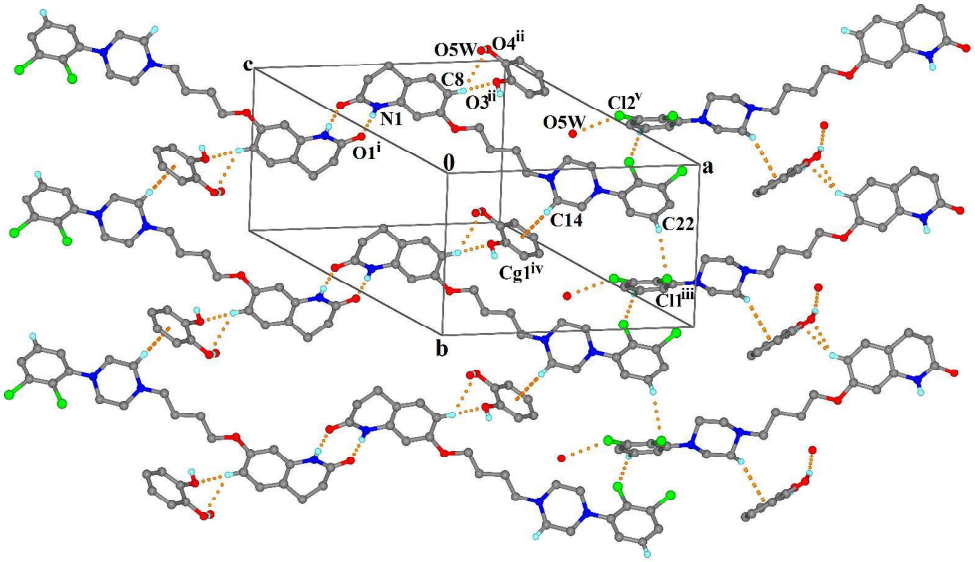

(a)

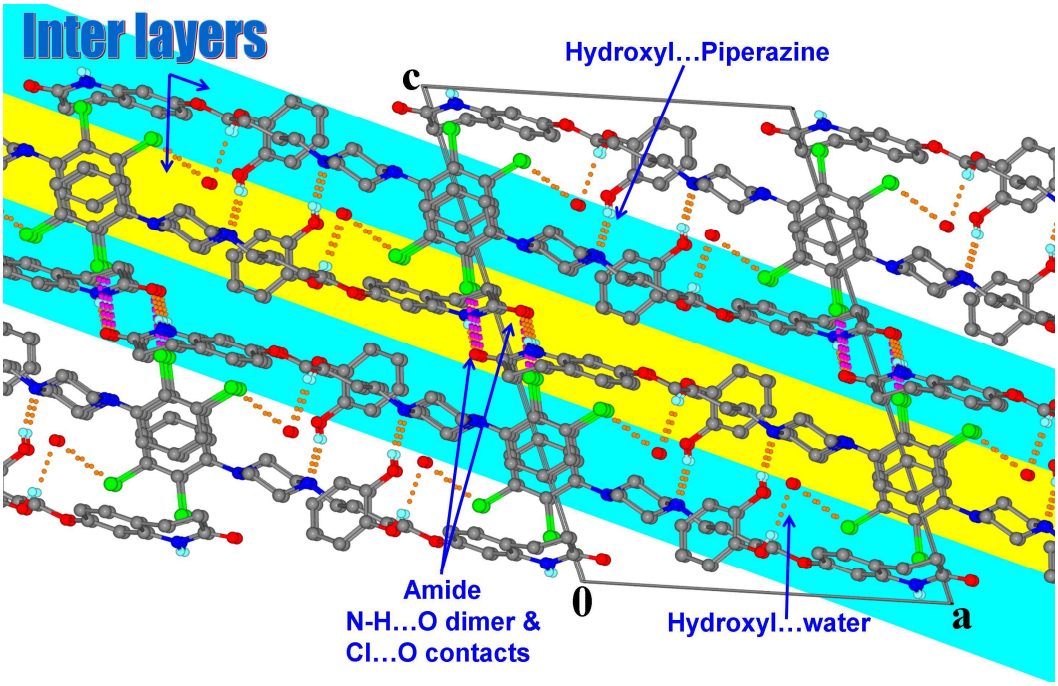

(b)

Fig. 8 (a) The centrosymmetric amide N1–H1···O1 dimer is extended into a 2D layered structure by a combination of C8–H8···O3, C8–H8···O4, C14–H14B···Cg1 and C22–H22···Cl1 interactions. Water hydrogen bonding with chlorine atom is also seen in the 2D layer. (b) Three dimensional interlayer bonding in cocrystal II is achieved through short Cl1···O1 contacts and hydroxyl…piperazine hydrogen bonds. Symmetry codes, [i] -x,-y,1-z; [ii] 1-x,-1/2+y,1/2-z; [iii] 2-x,1/2+y,1/2-z; [iv] 1-x,1/2+y,1/2-z; [v] 2-x,-1/2+y,1/2-z; [vi] 1-x, -y, 1-z; Cg1 is the centroid of C24-C29 atoms.

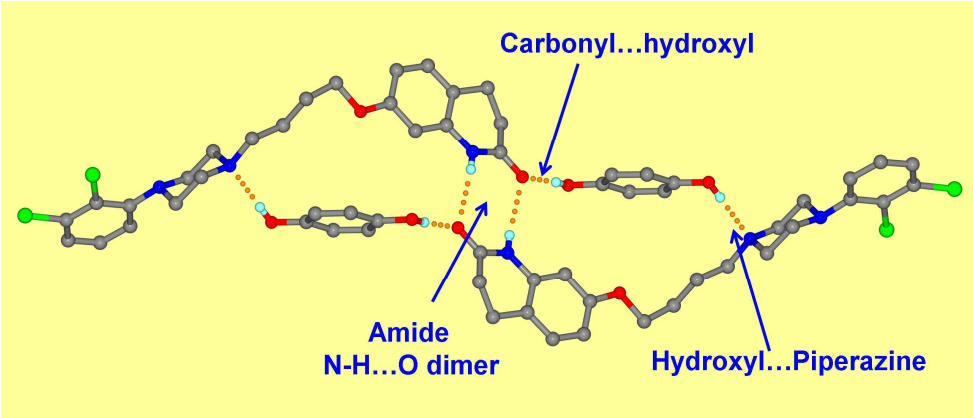

(a)

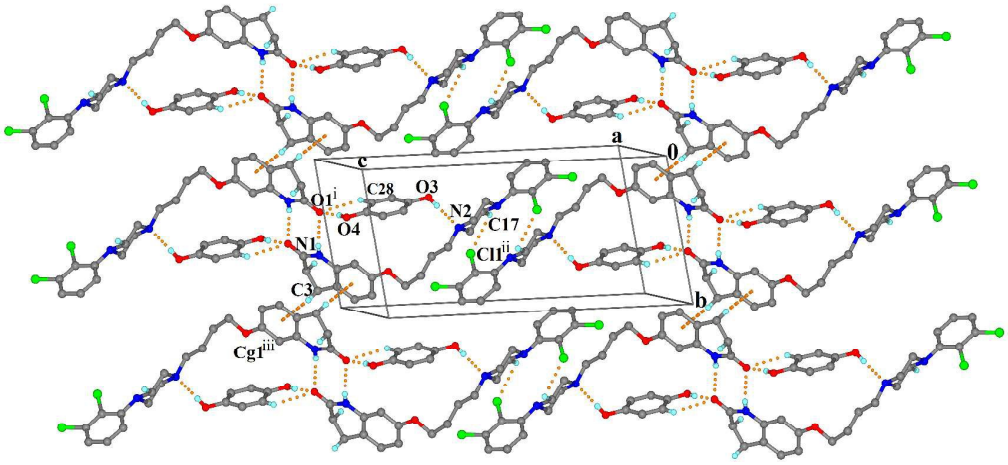

(b)

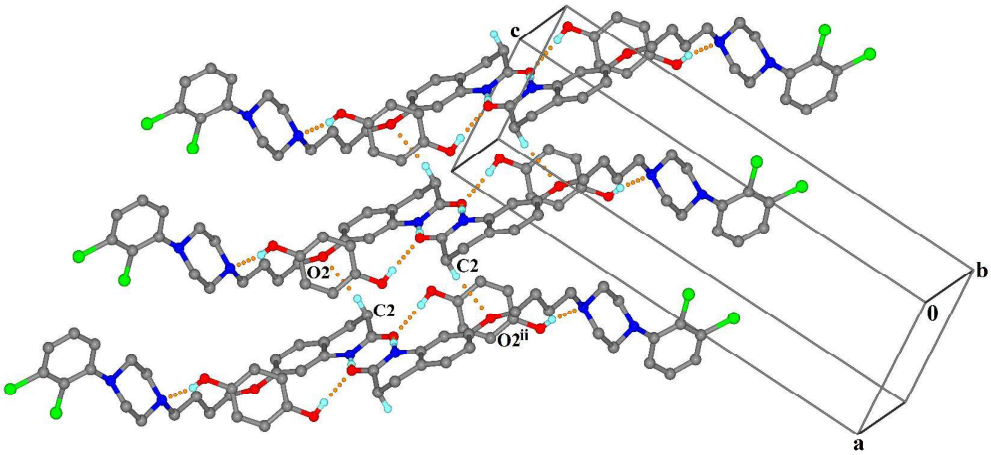

(c)

Fig. 9 (a) Utilization of all conventional hydrogen bonds, N1–H1···O1, O–H3O···N1 and O4–H4O···O1 interactions, for a discrete unit formation. (b) Propagation of the discrete unit into a 2D layer by C17–H17A···Cl1 and C3–H3B···Cg1 interactions. (c) Three dimensional crystal packing governed by C2–H2A···O2 interaction is shown. Symmetry codes, [i] 3-x,1-y,2-z; [ii] 1+x,y,z; [iii] 3-x,2-y,2-z.

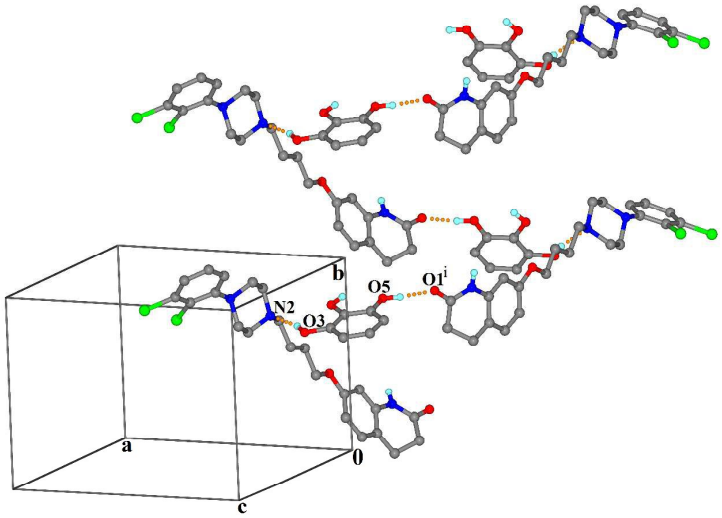

(a)

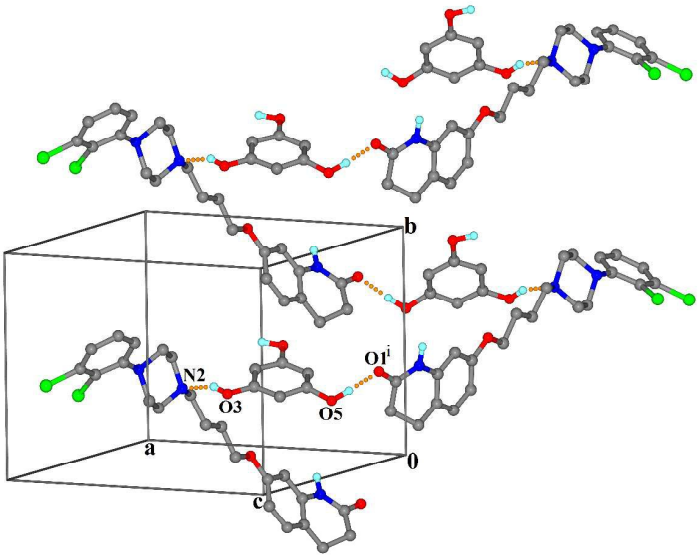

(b)

Fig. 10 (a) Helical propagation in cocrystal IV (b) Helical propagation in cocrystal V. Note that the coformers in I, IV and V have hydroxyls at 1 and 3-positions of aromatic ring which facilitates O–H3O···N1 and O5–H5O···O1 interactions and maintain isostructurality.

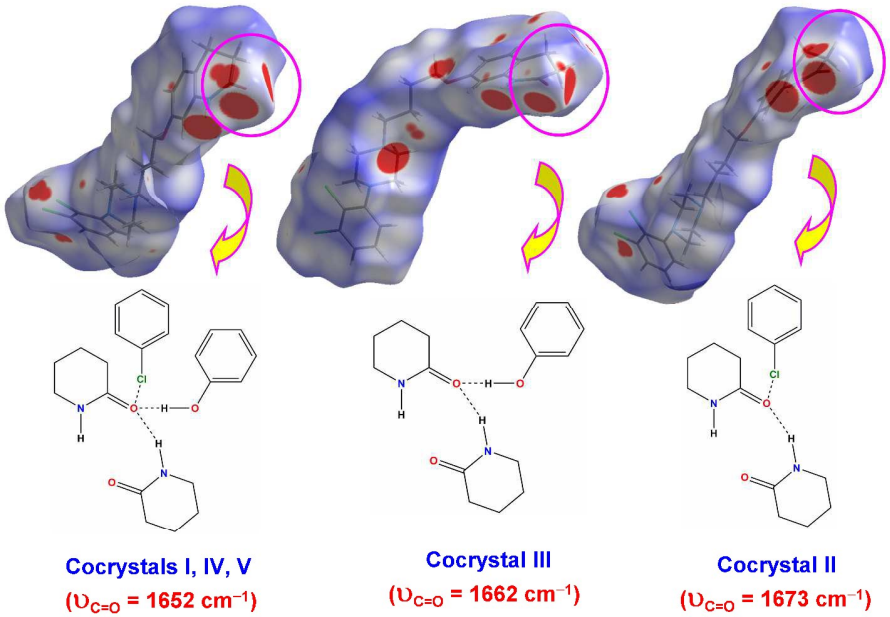

Fig. 11. The results of Hirshfeld surface analysis performed on aripiprazole molecule in cocrystals. The default d_{norm} property is mapped on to the surface. Hot red spots on the surfaces indicate intermolecular interactions. Cocrystals I, IV and V show three types of interactions (encircled region, three hot spots), whereas cocrystals II and III show only two types of interactions (two hot spots), which are shown schematically. The number of intermolecular contacts and their relative strengths are correlated well with the spectral shifts of C=O band.

Graphical Abstract

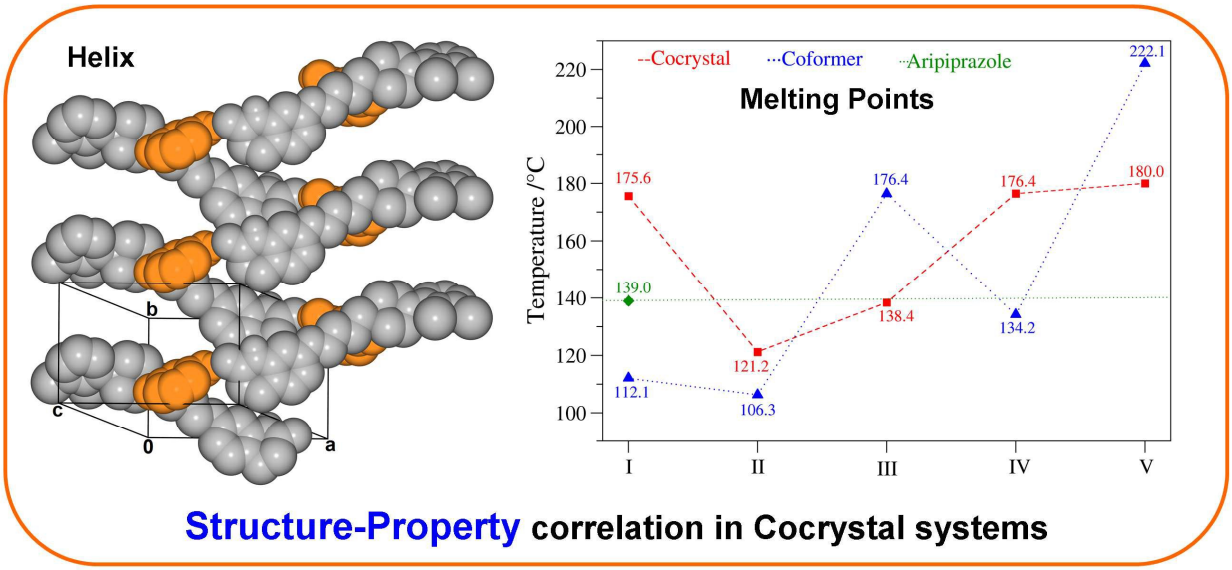

Structural reasons for the melting point variations in isostructural cocrystals of ariprazole drug are investigated through a combined spectroscopic and diffraction studies.